

Neural Phase Oscillator Representations of Behavioral Stimulus-Response Models

P. Suppes^a, J. Acacio de Barros^b, G. Oas^a

^a*CSLI, Ventura Hall, 220 Panama Street, Stanford University, Stanford, CA 94305-4101*

^b*Liberal Studies Program, San Francisco State University, 1600 Holloway Ave., San Francisco, CA 94132*

Abstract

The activity of a collection of neurons can be represented by weakly-coupled non-linear phase oscillators satisfying Kuramoto's equations. In this article, we build such neural-oscillator models, partly based on neurophysiological evidence, to represent approximately the learning behavior predicted and confirmed in several experiments by well-known stochastic learning models of behavioral stimulus-response theory.

Keywords: learning; neural oscillators; stimulus-response theory; phase representation; continuum of responses

1. Introduction

With the advent of modern experimental and computational techniques, substantial progress has been made in understanding the brain's mechanisms for learning. For example, extensive computational packages based on detailed experimental data on ion-channel dynamics make it now possible to simulate the behavior of networks of neurons starting from the flow of ions through the neuron's membrane (Bower and Beeman, 2003). Yet, there is much to be determined at a system level about brain processes. This can be contrasted to the large literature in psychology on learning, psychophysics, and perception. Among the most developed behavioral mathematical models of learning are those of stimulus-response (SR) theory (Bower, 1961; Estes et al., 1959; Suppes and Atkinson, 1960; Suppes and Ginsberg, 1963). (From the huge

Email addresses: psuppes@stanford.edu (P. Suppes), barros@sfsu.edu (J. Acacio de Barros), oas@stanford.edu (G. Oas)

SR literature, we reference here only the results we use in some detail.) In this article, we represent with neural oscillators some specific models of SR theory. We then analyze with oscillators two experiments, one on paired-associate learning and the other on probability matching, and the conditional probabilities for a continuum of responses.

The assumptions we make are broadly based on neurophysiological evidence. Neural oscillators, made up of collections of synchronized neurons are apparently ubiquitous in the brain, and their oscillations are macroscopically observable in electroencephalograms (Freeman, 1979; Gerstner and Kistler, 2002; Wright and Liley, 1995). Detailed theoretical analysis of weakly interacting neurons close to a bifurcation show oscillations (Gerstner and Kistler, 2002; Hoppensteadt and Izhikevich, 1996a,b; Izhikevich, 2007). Many experiments not only show the presence of oscillators in the brain (Eckhorn et al., 1988; Friedrich et al., 2004; Kazantsev et al., 2004; Lutz et al., 2002; Murthy and Fetz, 1992; Rees et al., 2002; Rodriguez et al., 1999; Sompolinsky et al., 1990; Steinmetz et al., 2000; Tallon-Baudry et al., 2001; Wang, 1995), but also that their synchronization is related to perceptual processing (Friedrich et al., 2004; Kazantsev et al., 2004; Leznik et al., 2002; Murthy and Fetz, 1992; Sompolinsky et al., 1990) and may play a role in solving the binding problem (Eckhorn et al., 1988). Neural oscillators have already been used to model a wide range of brain functions, such as pyramidal cells (Lytton and Sejnowski, 1991), effects of electric fields in epilepsy (Park et al., 2003), activities in the cat visual cortex (Sompolinsky et al., 1990), learning of songs by birds (Trevisan et al., 2005), and coordinated finger tapping (Yamanishi et al., 1980). Suppes and Han (2000) showed that a small number of frequencies can be used to recognize a verbal stimulus from EEG data, consistent with the brain representation of language being neural oscillators.

In our approach, each behavioral stimulus, response and reinforcement is represented by a neural oscillator satisfying Kuramoto’s nonlinear equations for phase oscillators (Acebron et al., 2005; Hoppensteadt and Izhikevich, 1996a,b; Kuramoto, 1984; Strogatz, 2000; Winfree, 2002). When a stimulus is sampled, its corresponding oscillator may phase lock to a response oscillator. When a reinforcement occurs, the coupling strengths change, driven by the reinforcement oscillator. Thus, SR conditioning is represented by phase locking driven by pairwise oscillator couplings, whose changes

reflect learning.

Despite the large number of models of processing in the brain, we know of no detailed systematic efforts to fit oscillator models to behavioral learning data. It is our goal in this paper to start bridging this gap. We choose to start with SR theory for several reasons. This theory has a solid mathematical foundation (Suppes, 2002); it has been used to predict many non-trivial quantitative features of learning, especially in the form of experimentally observed conditional probabilities (Suppes and Atkinson, 1960; Suppes and Ginsberg, 1963; Bower, 1961). It can also be used to represent computational structures, such as finite automata (Suppes, 2002). Furthermore, because neural oscillators can interfere (see, for example, our treatment of a continuum of responses below), they may provide a basis for quantum-like behavior in the brain (de Barros and Suppes, 2009; Suppes and de Barros, 2007), an area of intense research in recent years (Bruza et al., 2009).

We start with a brief review of SR theory. We next present in some detail the oscillator representation of the one-element SR model. Extension to other SR models follows. As already remarked, we end by comparing simulations of our oscillator models to behavioral data from two experiments.

2. Stimulus-Response Theory

Here is a verbal but axiomatic formulation of SR theory restricted to sampling a single stimulus pattern on each trial (Estes et al., 1959; Suppes and Atkinson, 1960). Calling the basic assumptions *axioms* is justified by the fact that this pattern approach has had many successful experimental applications (Suppes and Atkinson, 1960; Suppes and Ginsberg, 1963). For formal details and more general formulation of the theory, including sampling many stimulus components on the same trial, see Estes et al. (1959); Suppes (2002). Let n be the trial number, C_n be the state of conditioning at the beginning of trial n , S_n the sampled stimulus, R_n the response, and E_n the reinforcement, all on trial n . Each trial has the following temporal sequence of events:

$$C_n \rightarrow S_n \rightarrow R_n \rightarrow E_n \rightarrow C'_{n+1}, \quad (1)$$

where C'_{n+1} is the new state of conditioning at the beginning of trial $n + 1$.

Sampling Axioms.

- S1.** On every trial exactly one stimulus is randomly sampled from the finite presentation set.
- S2.** The probability of a particular sample on a trial, given the presentation set of stimuli, is independent of the trial number or any preceding pattern of events.

Conditioning and Reinforcement Axioms.

- C1.** On every trial each stimulus is conditioned to at most one response.
- C2.** The probability is c of any sampled stimulus becoming conditioned to the reinforced response if it is not already so conditioned, and this probability is independent of the particular response, trial number, or any preceding pattern of events.
- C3.** The conditioning of all stimuli remains the same if no response is reinforced, and the conditioning of unsampled stimuli does not change.

Response Axioms.

- R1.** If the sampled stimulus is conditioned to some response, then that response is made.
- R2.** If the sampled stimulus is not conditioned to any response, then the probability of any response is a constant guessing probability that is independent of the trial number and of any preceding pattern of events.

An important example is the *one-stimulus model* (often called in the earlier literature the *one-element model*), which we apply to paired-associate learning data. The two essential assumptions are the following. Until the single stimulus is conditioned, there is, first, a constant guessing probability p that the subject responds correctly (Axiom R2 above), and second, on each trial there is a constant probability c that the single stimulus will be conditioned to the reinforced response, if it is not already so conditioned (Axiom C2). These assumptions imply that there is a binomial distribution,

with parameter p , of the responses prior to the last error when exactly one response, and always the same one, is reinforced.

From the axioms just stated, we can also compute probabilistic features of many other SR models satisfying them. Here are four conditional probabilities for the N -stimulus model at asymptote for noncontingent reinforcement of R_1 with probability β and R_2 with probability $1 - \beta$, $0 < \beta < 1$, the standard reinforcement schedule for probability-matching experiments (Suppes and Atkinson, 1960). (In the SR literature π is used instead of β for the constant probability of reinforcement, but here we use π with its ordinary mathematical meaning.) The mean asymptotic probability of an R_1 response, independent of the number N of stimuli or the learning parameter, is β , i.e., $P_\infty(R_{1,n}) = \beta$, and

$$P_\infty(R_{1,n+1}|E_{1,n}R_{1,n}) = \beta + \frac{1 - \beta}{N}, \quad (2)$$

$$P_\infty(R_{1,n+1}|E_{1,n}R_{2,n}) = \beta \left(1 - \frac{1}{N}\right) + \frac{c}{N}, \quad (3)$$

$$P_\infty(R_{1,n+1}|E_{2,n}R_{1,n}) = \beta \left(1 - \frac{1}{N}\right) + \frac{1 - c}{N}, \quad (4)$$

$$P_\infty(R_{1,n+1}|E_{2,n}R_{2,n}) = \beta \left(1 - \frac{1}{N}\right). \quad (5)$$

We use these conditional probabilities, useful for estimating c and N , in analyzing the behavior of the relevant oscillator models.

The SR models above describe work well for many experimental situations where a finite number of responses is available to the subject (Bower, 1961; Estes et al., 1959; Estes and Suppes, 1959; Suppes and Atkinson, 1960). However, there are situations where a continuum of responses is necessary, and an extension of SR theory to account for such situations was developed by Suppes (1959). The idea is to represent conditioning by a smearing distribution $K(x; y)$, where y is the distribution's mean. When a stimulus conditioned to y is sampled, the response distribution density is given by $k(x; y)$. According to this model, for a noncontingent reinforcement with distribution density $f(y)$, the asymptotic probability of a response x is given by the density

$$r(x) = \int_a^b k(x; y)f(y)dy, \quad (6)$$

where $[a, b]$ is the interval of possible responses. Equation (6) can be used to estimate from experiments the characteristics of the smearing distribution (Suppes and Frankmann, 1961).

3. Oscillator Representations of Stimulus-Response Models

Before we discuss learning, let us focus on the representation of responses using oscillators. Intuitively, we are thinking of groups of self-sustaining neural oscillators. In the case of the one-element model, one of those oscillators corresponds to the stimulus, say oscillator O_s . In the case of two possible responses, two oscillators, O_{r_1} and O_{r_2} , represent each response. The idea behind our model is simple. O_{r_1} and O_{r_2} are, by themselves, unable to elicit a behavioral response, say, in the form of the activation of a set of muscles. However, if the firings of, say, O_{r_1} happens in synchrony with O_s , the extra firings of O_s push the activity of O_{r_1} above a threshold level, eliciting the activation of a response (i.e., the contraction of a muscle). Thus, oscillations of O_s and O_{r_1} becoming synchronized, while simultaneously O_s and O_{r_2} becoming out of sync, correspond to a behavioral response associated to the oscillator O_{r_1} .

Let us now look into the details of the model. In the N -stimulus oscillator model, restricted to two responses, each sampled stimulus is represented by one oscillator s_j ($j = 1, \dots, N$), the two possible responses by oscillators r_1 and r_2 , and reinforcements of r_1 and r_2 by oscillators e_1 and e_2 (to avoid confusion, whenever possible we will use lower-case letters for oscillators, e.g. response oscillator r_1 , and upper-case for SR concepts, e.g. response R_1). At the beginning of an experiment, we assume all the oscillators mentioned are connected by at least weak random couplings. This is a reasonable model assumption, even though empirical support may be difficult to find in the current literature. (This assumption is analogous to assigning a positive prior probability, no matter how small, to all relevant hypotheses for the purpose of Bayesian analysis.) When a stimulus S_n is sampled with probability $1/N$, we assume its corresponding phase oscillator s_j activates, i.e., the neurons of this oscillator start to fire synchronously. This activation is followed by the spreading of activation to the two response oscillators. After any given time interval, the dynamics leads to changes in the phase relations between the stimulus and the response oscillators. Depending on the

couplings, the stimulus and response oscillators may phase lock with fixed phase relations. Two oscillators are phase locked if they keep a constant phase relation between each other (for a precise mathematical definition of phase locking, see Izhikevich and Kuramoto (2006)). In this way, depending on the couplings, after a finite amount of time one response may become in phase with the stimulus while the other dephases. The response then made is the one represented by the response oscillator whose phase is closest to s_j . Once again, we may think of this synchronicity as selecting an answer in the following way. If all oscillators, each representing several firing neurons, are synchronous, the activity level within a window of time may reach a certain threshold, and elicit a response. This phase coherence may correspond to the spatial coherence of bursts in the brain (Eckhorn et al., 1988; Fell et al., 2001; Freeman and Barrie, 1994; Rees et al., 2002; Sompolinsky et al., 1990; Varela et al., 2001).

Shortly after a response, during reinforcement, we assume that a neural oscillator representing the reinforcement disrupts the dynamics of the stimulus and response oscillators, forcing them to phase lock to the reinforcement oscillator with a phase difference of up to π and to change their couplings accordingly (for experimental evidence of phase shifts, see references in Ermentrout and Kleinfeld (2001)). The new reinforced couplings may result in a dynamics that yields new phase relationships between oscillators, thus changing the response to a stimulus. This sequence of neural events closely follows the sequence of behavioral events shown in (1), and loosely corresponds to a Hebbian learning rule.

We now turn to the mathematical description of these qualitative ideas. We assume that stimulus and response neural oscillators have natural frequencies ω_0 , such that their phases are $\varphi(t) = \omega_0 t + \text{constant}$, when they are not interacting with other oscillators. We also assume that they are weakly coupled to each other with symmetric couplings. The assumption of coupling between response oscillators is a detailed feature that has no direct correspondence in the SR model. Let $t_{s,n}$ be the time at which the stimulus oscillator is activated on trial n and Δt_r the mean amount of time it takes for a response oscillator to phase lock. The assumption of the same frequency for stimulus and response oscillators is not necessary, as oscillators with different natural frequency can entrain (Kuramoto, 1984), but it simplifies our analysis, as we focus on phase lock-

ing. In a real biological system, however, we should expect different neural oscillators to have different frequencies.

At the beginning of a trial, a stimulus is sampled, and once its corresponding oscillator, s_j , along with r_1 and r_2 , are activated, the phase of each oscillator resets according to a normal distribution centered on zero, i. e., $\bar{\varphi} = 0$, with standard deviation σ_φ , which is the same for all stimulus and response oscillators. (We chose $\bar{\varphi} = 0$ without loss of generality, since only phase differences are physically meaningful. The Gaussian is used to represent biological variability. A possible mechanism for this phase reset can be found in Wang (1995).) Independently of n , the probability density for the phase at time $t_{s,n}$ is given by

$$f(\varphi_i) = \frac{1}{\sigma_\varphi \sqrt{2\pi}} \exp\left(-\frac{\varphi_i^2}{2\sigma_\varphi^2}\right), \quad (7)$$

where $i = s_j, r_1, r_2$. After the stimulus is sampled, the three active oscillators evolve for the time interval Δt_r according to the following set of differential equations, known as the Kuramoto equations (Hoppensteadt and Izhikevich, 1996a,b; Kuramoto, 1984).

$$\begin{aligned} \frac{d\varphi_{s_j}}{dt} = & \omega_0 - k_{s_j,r_1} \sin(\varphi_{s_j} - \varphi_{r_1}) \\ & - k_{s_j,r_2} \sin(\varphi_{s_j} - \varphi_{r_2}), \end{aligned} \quad (8)$$

$$\begin{aligned} \frac{d\varphi_{r_1}}{dt} = & \omega_0 - k_{s_j,r_1} \sin(\varphi_{r_1} - \varphi_{s_j}) \\ & - k_{r_1,r_2} \sin(\varphi_{r_1} - \varphi_{r_2}), \end{aligned} \quad (9)$$

$$\begin{aligned} \frac{d\varphi_{r_2}}{dt} = & \omega_0 - k_{s_j,r_2} \sin(\varphi_{r_2} - \varphi_{s_j}) \\ & - k_{r_1,r_2} \sin(\varphi_{r_2} - \varphi_{r_1}), \end{aligned} \quad (10)$$

where φ_{s_j} , φ_{r_1} , and φ_{r_2} are their phases, ω_0 their natural frequency, and $k_{s_1,r_1}, \dots, k_{s_N,r_2}, k_{r_1,r_2}$ are the $2N + 1$ coupling strengths between oscillators. Equations (8)–(10) usually contain the amplitudes of the oscillators as a coupling factor. For instance, instead of just k_{s_j,r_1} in (8), the standard form of Kuramoto's equation would have a $A_{s_j} A_{r_1} k_{s_j,r_1}$ term multiplying $\sin(\varphi_{s_j} - \varphi_{r_1})$ (Kuramoto, 1984). For simplicity, we omit this term. However, we could think of amplitudes as a mechanism for oscillator activation, as an amplitude proportional to $A \cos(\varphi_{s_j} - \varphi_{r_1})$ could strengthen the coupling of in-phase oscillators. It would be desirable to develop a dynamic theory of spreading activation,

but this would go beyond the scope of this paper. Before any conditioning, the values for the coupling strengths are chosen following a normal distribution $g(k)$ with mean \bar{k} and standard deviation σ_k . It is important to note that reinforcement will change the couplings while the reinforcement oscillator is acting upon the stimulus and response oscillators, i.e. during Δt_r , according to the set of differential equations presented later in this section. The solutions to (8)–(10) and the initial conditions randomly distributed according to $f(\varphi_i)$ give us the phases at time $t_{r,n} = t_{s,n} + \Delta t_r$. (Making Δt_r a random variable rather than a constant is a realistic generalization of the constant value we have used in computations.) The coupling strengths between oscillators determine their phase locking and how fast it happens. If a stimulus oscillator phase-locks in phase to a response oscillator, this represents in SR theory that the stimulus is conditioned to that response, but we do not require precise phase locking between the stimulus and response oscillators. More accurately, the oscillator representing the response at trial n is the oscillator whose actual phase difference at time $t_{r,n}$ is the smaller with respect to s_j , i.e., the smaller c_i ,

$$c_i - \pi = |\varphi_{r_i} - \varphi_{s_j} - \pi| \bmod 2\pi, \quad i = 1, 2. \quad (11)$$

To better understand (8)–(10), let us rewrite them in terms of the phase differences, since this is all that matters.

$$\begin{aligned} \frac{d\phi_{1j}}{dt} &= -2k_{s_j,r_1} \sin(\phi_{1j}) - k_{s_j,r_2} \sin(\phi_{2j}) \\ &\quad - k_{r_1,r_2} \sin(\phi_{1j} - \phi_{2j}), \end{aligned} \quad (12)$$

$$\begin{aligned} \frac{d\phi_{2j}}{dt} &= -k_{s_j,r_1} \sin(\phi_{1j}) - 2k_{s_j,r_2} \sin(\phi_{2j}) \\ &\quad + k_{r_1,r_2} \sin(\phi_{1j} - \phi_{2j}), \end{aligned} \quad (13)$$

where $\phi_{1j} = \varphi_{r_1} - \varphi_{s_j}$ and $\phi_{2j} = \varphi_{r_2} - \varphi_{s_j}$. Equations (12) and (13) have the following fixed points: (i) $\phi_{1j} = \phi_{2j} = 0$, (ii) $\phi_{1j} = \pi$, $\phi_{2j} = 0$, and (iii) $\phi_{1j} = 0$, $\phi_{2j} = \pi$. For typical biological parameters and the physical ones we have added, the rate of convergence is such that the solutions to (12) and (13) are well approximated by the asymptotic fixed points by the time a response is made. But given that we have three

different fixed points, how can r_1 be the conditioned response oscillator (fixed point iii) if r_2 can also phase-lock in phase (fixed point ii)?

To answer this question, we examine the stability of these fixed points, i.e., whether small changes in the initial conditions for the phases lead to the same phase differences. In the Appendix A we linearize (12) and (13) for small fluctuations around each fixed point. As shown there, a sufficient condition for fixed point $(0, \pi)$ to be stable is:

$$k_{s_j, r_2} k_{r_1, r_2} > k_{s_j, r_1} k_{s_j, r_2} + k_{s_j, r_1} k_{r_1, r_2}$$

and the other fixed points unstable (see Fig. 1). It is important to emphasize that, although the above result shows asymptotic stability, it does not imply synchronization within a fixed finite time. Because neural oscillators need to operate in rather small amounts of time, numerical simulations are necessary to establish synchronization.

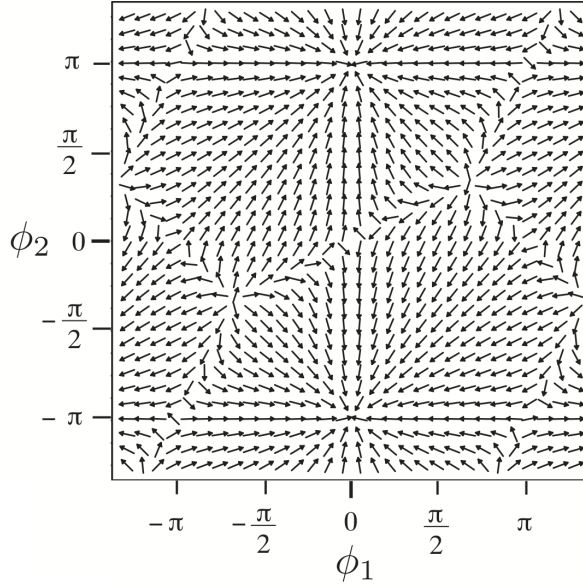


Figure 1: Field plot, generated using Maple 10, for couplings $k_{s_j, r_1} = k_{r_1, r_2} = -k$ and $k_{s_j, r_2} = k$, $k > 0$. Field lines show that the fixed point at $(0, \pi)$ is stable, whereas $(0, 0)$, $(\pi, 0)$, (π, π) , $(\pi/3, 2\pi/3)$, and $(2\pi/3, \pi/3)$ are unstable. Thus, for a randomly selected initial condition, in a finite amount of time s_j approaches the phase of r_1 and departs from r_2 .

If the couplings are zero, the model still picks one of the oscillators: the one with the

minimum value for c_i in (11). But in this case, because of the small fluctuations in the initial conditions, the probability for each response is $1/2$, as expected, corresponding, obviously, to the SR parameter $p = 1/2$.

In SR theory, learning occurs through changes in conditioning when a reinforcement occurs. E_n , the reinforcement random variable, can take values 1 and 2 in our current example. If $E_n = 1$ ($E_n = 2$), the corresponding reinforcement oscillator e_1 (e_2) activates, interacting with the stimulus and response oscillators in a way described below. A reinforcement is a strong external event that drives all active oscillators to synchronize with frequency ω_e to the reinforcement oscillator, while phase locking to it. We choose $\omega_e \neq \omega_0$ to keep its role explicit in our computations. In (8)–(10) there is no reinforcement, and we assume that prior to any reinforcement, i.e., for $t < t_{e,1}$, the couplings $k_{s_1,r_1}, \dots, k_{s_N,r_2}$ are normally distributed with mean \bar{k} and standard deviation σ_k . To develop equations for conditioning, we assume that when reinforcement is effective, the reinforcement oscillator deterministically interferes with the evolution of the other oscillators. This is done by assuming that the reinforcement event forces the reinforced response and the stimulus oscillator to synchronize with the same phase, while the other response oscillator synchronizes in a phase difference of $\pi/2$ (anti-phase). Let a reinforcement oscillator be activated on trial n at time $t_{e,n}$, $t_{r,n+1} > t_{e,n} > t_{r,n}$, during an interval Δt_e . Let K_0 be the coupling strength between the reinforcement oscillators and the stimulus and response oscillators. In order to match the probabilistic SR axiom governing the effectiveness of reinforcement, we assume, as something beyond Kuramoto's equations, that there is a normal probability distribution governing the coupling strength K_0 between the reinforcement and the other active oscillators. It has mean \bar{K}_0 and standard deviation σ_{K_0} . Its density function is:

$$f(K_0) = \frac{1}{\sigma_{K_0} \sqrt{2\pi}} \exp \left\{ -\frac{1}{2\sigma_{K_0}^2} (K_0 - \bar{K}_0)^2 \right\}. \quad (14)$$

As already remarked, a reinforcement is a disruptive event. When it is effective, all active oscillators phase-reset at $t_{e,n}$, and during reinforcement the phases and the couplings of the active oscillators evolve according to the following set of differential equa-

tions.

$$\begin{aligned} \frac{d\varphi_{s_j}}{dt} = & \omega_0 - k_{s,r_1} \sin(\varphi_{s_j} - \varphi_{r_1}) - k_{s_j,r_2} \sin(\varphi_{s_j} - \varphi_{r_2}) \\ & + K_0 \sin(\varphi_{s_j} - \omega_e t), \end{aligned} \quad (15)$$

$$\begin{aligned} \frac{d\varphi_{r_1}}{dt} = & \omega_0 - k_{s_j,r_1} \sin(\varphi_{r_1} - \varphi_{s_j}) - k_{r_1,r_2} \sin(\varphi_{r_1} - \varphi_{r_2}) \\ & + K_0 \sin(\varphi_{r_1} - \omega_e t - \pi(1 - \delta_{e_n,1})), \end{aligned} \quad (16)$$

$$\begin{aligned} \frac{d\varphi_{r_2}}{dt} = & \omega_0 - k_{s_j,r_2} \sin(\varphi_{r_2} - \varphi_{s_j}) - k_{r_1,r_2} \sin(\varphi_{r_2} - \varphi_{r_1}) \\ & + K_0 \sin(\varphi_{r_2} - \omega_e t - \pi(1 - \delta_{e_n,2})), \end{aligned} \quad (17)$$

$$\frac{dk_{s_j,r_1}}{dt} = \epsilon(K_0) [\alpha \cos(\varphi_{s_j} - \varphi_{r_1}) - k_{s_j,r_1}], \quad (18)$$

$$\frac{dk_{s_j,r_2}}{dt} = \epsilon(K_0) [\alpha \cos(\varphi_{s_j} - \varphi_{r_2}) - k_{s_j,r_2}], \quad (19)$$

$$\frac{dk_{r_1,r_2}}{dt} = \epsilon(K_0) [\alpha \cos(\varphi_{r_1} - \varphi_{r_2}) - k_{r_1,r_2}], \quad (20)$$

where

$$\epsilon(K_0) = \begin{cases} 0 & \text{if } K_0 < K' \\ \epsilon_0 & \text{otherwise,} \end{cases} \quad (21)$$

$\delta_{e_n,1}$ and $\delta_{e_n,2}$ are Kronecker's delta, $\epsilon_0 \ll \omega_0$, α and K_0 are constant during Δt_e (Hoppensteadt and Izhikevich, 1996a,b), and K' is a threshold constant throughout all trials. The function $\epsilon(K_0)$ represents nonlinear effects in the brain. These effects could be replaced by the use of a sigmoid function $\epsilon_0(1 + \exp\{-\gamma(K_0 - K')\})^{-1}$ (Eeckman and Freeman, 1991) in (18)–(20), but we believe that our current setup makes the probabilistic features clearer. In both cases, we can think of K' as a threshold below which the reinforcement oscillator has no (or very little) effect on the stimulus and response oscillators.

Before we proceed, it is worthwhile to analyze qualitatively the dynamical (15)–(20) (for details, see the Appendix A). Equations (15)–(17) are simply (8)–(10) with an extra driving term from an external source with frequency ω_e , the reinforcement oscillator. The disruptive event $e_n = 1$ produces the phase difference term $\pi(1 - \delta_{e_n,1}) = 0$ for r_1 and $\pi(1 - \delta_{e_n,2}) = \pi$ for r_2 , and similarly for $e_n = 2$, namely, π and 0 for r_1 and r_2 , respectively. If the last term in (15)–(17) dominates the others, i.e., if $K_0 \gg \omega_0$ and $K_0 \gg k$ for all $k \in \{k_{s_1,r_1}, \dots, k_{s_N,r_2}, k_{r_1,r_2}\}$, then the corresponding oscillators

converge to the same frequency as the driving term. For example, let $E_n = 1$, and let us approximate (15)–(17) by eliminating terms that are small compared to K_0 :

$$\frac{d\varphi_{s_j}}{dt} = \omega_0 + K_0 \sin(\varphi_{s_j} - \omega_e t), \quad (22)$$

$$\frac{d\varphi_{r_1}}{dt} = \omega_0 + K_0 \sin(\varphi_{r_1} - \omega_e t), \quad (23)$$

$$\frac{d\varphi_{r_2}}{dt} = \omega_0 + K_0 \sin(\varphi_{r_2} - \omega_e t - \pi). \quad (24)$$

It is straightforward to show that the solutions for (22)–(24) converge, for $t > 2/\sqrt{K_0^2 - (\omega_e - \omega_0)^2}$ and $K_0^2 \gg (\omega_0 - \omega_e)^2$, to $\varphi_{s_j} = \varphi_{r_1} = \omega_e t - \pi$ and $\varphi_{r_2} = \omega_e t$ if $\omega_e \neq \omega_0$. So, the effect of the new terms added to Kuramoto's equations is to force a specific phase synchronization between s_j , r_1 , and r_2 , and the activated reinforcement oscillator, which is either e_1 or e_2 .

We next turn to the coupling (18)–(20). For $K_0 > K'$ and $E_n = 1$, φ_{s_j} and φ_{r_1} evolve, approximately, to $\omega_e t + \pi$, and φ_{r_2} to $\omega_e t$. Thus, k_{s_j, r_1} in (18) tends to a solution of the form $\alpha + c_1 \exp(-\epsilon_0 t)$ whereas k_{s_j, r_2} and k_{r_1, r_2} in (19) and (20) tend to $-\alpha + c_2 \exp(-\epsilon_0 t)$, with c_1 and c_2 being integration constants. For a finite time $t > 1/\epsilon_0$ those values satisfy the stability requirements shown above.

The phase differences between stimulus and response oscillators are determined by which reinforcement oscillator is driving the changes to the couplings during learning. From (18)–(20), reinforcement may be effective only if $\Delta t_e > \epsilon_0^{-1}$ (see Seliger et al. (2002) and Appendix C), setting a lower bound for ϵ_0 , as Δt_e is fixed by the experiment. For values of $\Delta t_e > \epsilon_0^{-1}$, the behavioral probability parameter c of effective reinforcement is, from (14) and (21), reflected in the oscillator representation by the equation:

$$c = \int_{K'}^{\infty} f(K_0) dK_0. \quad (25)$$

This relationship comes from the fact that if $K_0 < K'$, there is no effective reinforcement, since there are no changes to the couplings due to (18)–(20), and (8)–(10) describe the oscillators' behavior (more details can be found in Appendix C). Intuitively K' is the effectiveness parameter. The larger it is, relative to $\overline{K_0}$, the smaller the probability the random value K_0 of the coupling will be effective by changing the values of the couplings through (18)–(20).

Equations (15)–(20) are similar to the evolution equations for neural networks, derived from some reasonable assumptions in Hoppensteadt and Izhikevich (1996a,b). The general idea of oscillator learning similar to (15)–(20) was proposed in Seliger et al. (2002) and Nishii (1998) as possible learning mechanisms.

3.1. Parameter values

We turn now to the parameters used in our oscillator models. In the above equations, we have as parameters N , ω_0 , ω_e , α , Δt_r , Δt_e , \bar{k} , σ_k , $\bar{\varphi}$, σ_φ , ϵ_0 , \bar{K}_0 , σ_{K_0} , and K' . This large number of parameters stands in sharp contrast to the small number needed for SR theory, which is abstract and therefore much simpler. In our view, any other detailed physical model of SR theory will face a similar problem. Experimental evidence constrains the range of values for ω_0 , ω_e , Δt_r , and Δt_e , and throughout this paper we choose $\omega_0 = 10$ Hz, $\omega_e = 12$ Hz, $\Delta t_r = 200$ ms, and $\Delta t_e = 400$ ms. These natural frequencies were chosen because: (i) they are in the lower range of frequencies measured for neural oscillators (Freeman and Barrie, 1994; Friedrich et al., 2004; Kazantsev et al., 2004; Murthy and Fetzi, 1992; Suppes and Han, 2000; Tallon-Baudry et al., 2001), and the lower the frequency, the slower the time it takes for two oscillators to synchronize, which imposes a lower bound on the time taken to make a response, (ii) data from Suppes et al. (1997, 1998, 1999b,a); Suppes and Han (2000) suggest that most frequencies used for the brain representation of language are close to 10 Hz, and (iii) choosing a small range of frequencies simplifies the oscillator behavior. We use $\Delta t_r = 200$ ms, which is consistent with the part it plays in the behavioral response times in many psychological experiments; for extended analysis of the latter see Luce (1986). The value for $\Delta t_e = 400$ ms is also consistent with psychological experiments.

Before any conditioning, we should not expect the coupling strengths between oscillators to favor one response over the other, so we set $\bar{k} = 0$ Hz. The synchronization of oscillators at the beginning of each trial implies that their phases are almost the same, so for convenience we use $\bar{\varphi} = 0$. The standard deviations σ_k and σ_φ are not directly measured, and we use for our simulations the reasonable values of $\sigma_k = 10^{-3}$ Hz and $\sigma_\varphi = \pi/4$ Hz. Those values were chosen because σ_k should be very small, since it is related to neuronal connections before any conditioning, and σ_φ should allow for a

measurable phase reset at the presentation of a stimulus, so $\sigma_\varphi < 1$.

The values of α , ϵ_0 , \bar{K}_0 , and σ_{K_0} are based on theoretical considerations. As we discussed in the previous paragraph, \bar{K}_0 is the mean strength for the coupling of the reinforcement oscillator, and σ_{K_0} is the standard deviation of its distribution. We assume in our model that this strength is constant during a trial, but that it varies from trial to trial according to the given probability distribution. The parameter α is related to the maximum strength allowed for the coupling constants k_{s_j, r_1} , k_{s_j, r_2} , and k_{r_1, r_2} . Because of the stability conditions for the fixed points, shown above, any value of α leads to phase locking, given enough time. The magnitude of α is monotonically related to how fast the system phase locks. It needs to be at least of the order of $1/\Delta t_r$ if the oscillators are to phase lock within the behavioral response latency. Another important parameter is ϵ_0 , and we can see its role by fixing the phases and letting the system evolve. In this situation, the couplings converge exponentially to α with a characteristic time ϵ_0^{-1} , so ϵ_0 determines how fast the couplings change. The time of response, Δt_r , given experimentally, sets a minimum value of 5 Hz for α , since $\alpha > \Delta t_r^{-1} = 5$ Hz is needed to have phase locking from Kuramoto-type equations. The time of reinforcement, Δt_e , and natural frequency ω_0 are related to ϵ_0 by $\epsilon_0 > \Delta t_e^{-1} = 2.5$ Hz and $\epsilon_0 \ll \omega_0$. Finally, to have an effective reinforcement, K_0 must satisfy $K_0 \gg \omega_0$. These theoretical considerations are consistent with the values $\alpha = 10$ Hz, $\epsilon_0 = 3$ Hz, $\bar{K}_0 = 90$ Hz, and $\sigma_{K_0} = 10$ Hz. We note one distinction about the roles of the three probability distributions introduced. Samples are drawn of phases φ and reinforcement oscillator coupling strength K_0 on each trial, but oscillator couplings $k_{s_1, r_1}, \dots, k_{s_N, r_2}, k_{r_1, r_2}$ are sampled only once at the beginning of a simulated experiment and then evolve according to (18)–(20).

Table

Table 1: Fixed values of parameters used to fit our oscillator models to SR experiments.

Parameter	Value	Parameter	Value
α	10 Hz	σ_φ	$\pi/4$
ω_0	10 Hz	\bar{k}	0 Hz
ω_e	12 Hz	σ_k	10^{-3} Hz
Δt_r	200 ms	σ_{K_0}	10 Hz
Δt_e	400 ms	\bar{K}_0	90 Hz
$\bar{\varphi}$	0	ϵ_0	3 Hz

1 summarizes the fixed parameter values used in our simulations, independent of considering the experimental design or data of a given SR experiment. This leaves us with two remaining free parameters to estimate from SR experimental data: the number of stimulus oscillators N and the non-linear cutoff parameter K' . These two parameters have a straightforward relation to the SR ones. N corresponds to the number of stimuli, and K' is monotonically decreasing with the effectiveness of reinforcement probability c , as shown in (25).

Fig. 2 exemplifies the phase-difference behavior of three oscillators satisfying Kuramoto's equations.

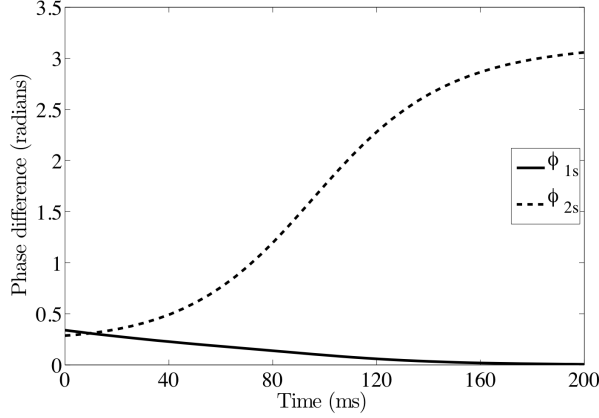


Figure 2: MATLAB computation of the phase differences between three coupled oscillators evolving according to Kuramoto's equations with couplings $k_{s_j, r_1} = \omega_0 = -k_{s_j, r_2} = k_{r_1, r_2}$ and $\omega_0 = 20\pi \text{ s}^{-1}$ (10 Hz). The solid line represents $\phi_{1s_j} = \varphi_{r_1} - \varphi_{s_j}$, and the dashed $\phi_{2s_j} = \varphi_{r_2} - \varphi_s$.

In the figure, as shown, all oscillators start with similar phases, but at 200 ms both s_j and r_1 lock with the same phase, whereas r_2 locks with phase difference π . Details on the theoretical relations between parameters can be found in Appendices B and C.

3.2. Continuum of Responses

We saw above how to describe a finite number of stimuli and responses using phase oscillators. In this section we extend the model to a continuum of responses. According to our model, conditioning to response r_1 leads to φ_{r_1} phase locking with the same phase as φ_s , whereas φ_{r_2} phase locks off by $\pi/2$. We justified this by relating synchronization with firing thresholds that could activate motor responses. For a continuum

of responses, we need to think not only of how to select a single response, but an infinite number of them. A way would be to postulate several response oscillators, each corresponding to a point in the continuum. With a large enough number of oscillators, such model could accommodate any experimental condition. However, it is improbable that the brain approximates the continuum by increasing the number of potential responses. We believe a more elegant approach, with a natural interpretation in terms of the underlying neurophysiology, is the use of phase differences by oscillators.

Let us start with three harmonic oscillators, O_s , O_{r_1} , and O_{r_2} , having the same natural frequency ω_0 . We further assume that once activated, O_s , O_{r_1} , and O_{r_2} have the same intensity. Then, we can write that

$$s(t) = k \cos(\omega_0 t) = k \cos(\varphi_s(t)), \quad (26)$$

$$r_1(t) = k \cos(\omega_0 t + \delta\phi_1) = k \cos(\varphi_{r_1}(t)), \quad (27)$$

$$r_2(t) = k \cos(\omega_0 t + \delta\phi_2) = k \cos(\varphi_{r_2}(t)), \quad (28)$$

where $s(t)$, $r_1(t)$, and $r_2(t)$ represent the harmonic oscillations of O_s , O_{r_1} , and O_{r_2} , $\varphi_s(t)$, $\varphi_{r_1}(t)$, and $\varphi_{r_2}(t)$ their phases, and $\delta\phi_1$ and $\delta\phi_2$ are constants. Notice that, since all oscillators have the same intensity, the dynamics is completely encoded in the phases.

Here we focus on the physical interpretation of the oscillations, and, to help this, we keep the full form (26)–(28). Since neural oscillators have a wave-like behavior (see Izhikevich (2007)), their dynamics satisfy the principle of superposition, and we can think of the response as an interference effect between O_s and the O_{r_1} , and O_{r_2} . As such, the mean intensity of the oscillations give us a measure of the excitation carried by the oscillations. To see how this corresponds to a continuum of responses, let O_{r_1} be an oscillator corresponding to the connections to a muscle M_1 , or perhaps even another set of oscillators. The intensity I_1 at M_1 is the superposition of $s(t)$ and $r_1(t)$, and we have

$$\begin{aligned} I_1 &= \langle (s(t) + r_1(t))^2 \rangle_t \\ &= \langle s(t)^2 \rangle_t + \langle r_1(t)^2 \rangle_t + \langle 2s(t)r_1(t) \rangle_t, \end{aligned}$$

where $\langle \rangle_t$ is the time average, and where we are assuming that the amplitudes of O_s and

O_{r_1} are the same at M_1 . A quick computation gives

$$I_1 = 1 + \cos(\delta\phi_1),$$

and, similarly for I_2 ,

$$I_2 = 1 + \cos(\delta\phi_2).$$

Therefore, the intensity depends on the phase difference between the oscillator itself and the stimulus oscillator. Before any learning, intensities I_1 and I_2 are uncorrelated, mainly because of the weak couplings between oscillators, as in the case of the one-element model.

After learning, one possibility is for O_{r_1} and O_{r_2} to become diametrically opposed responses (such as a two-response experiment). If we call I_1^L and I_2^L the intensities at M_1 and M_2 after learning, it is reasonable to assume that if I_1^L has maximum intensity, I_2^L has minimum intensity, and vice-versa. Thus, we are left with $I_{1,max}^L = 1 + \cos(0) = 1$ and $I_{2,min}^L = 1 + \cos(\pi) = 0$, or $I_{1,min}^L = 1 + \cos(\pi) = 0$ and $I_{2,max}^L = 1 + \cos(0) = 1$. This maximum contrast between responses happens when we impose $\delta\phi \equiv \delta\phi_1 = \delta\phi_2 + \pi$, as we had for the case of a two-response system, which results in

$$I_1^L = 1 + \cos(\delta\phi), \quad (29)$$

and

$$I_2^L = 1 - \cos(\delta\phi). \quad (30)$$

To obtain an arbitrary value as response, let us start with $b \in [-1, 1]$, and set it as the normalized difference in intensities between O_{r_1} and O_{r_2} , i.e.

$$b = \frac{I_1^L - I_2^L}{I_1^L + I_2^L} = \cos(\delta\phi), \quad (31)$$

$0 \leq \delta\phi \leq \pi$. This setup has natural correlates with behavioral responses. Say I_1 is the intensity at a muscle M_1 pulling an animal to response 1 on a scale from -1 to 1 , whereas I_2 is the intensity at M_2 pulling toward response -1 . The balance between M_1 and M_2 will determine how close the response will be to either 1 or -1 , and b is exactly a measure of such balance. If we reinforce $\delta\phi = 0$, we get $b = 1$; if we reinforce $\delta\phi = \pi$, $b = -1$; if we reinforce $\delta\phi = \arccos(b)$, we can obtain any value $b \in [-1, 1]$.

So, in principle we can use arbitrary phase differences between oscillators to code for a continuum of responses between -1 and 1 . For arbitrary intervals (ζ_1, ζ_2) , all that would be required is a re-scaling of b .

We now want to make sure that we can represent any phase difference $\delta\varphi$ by Kuramoto oscillators. For oscillators to synchronize with any phase relation, it is often proposed to modify Kuramoto's equations to the form

$$\dot{\varphi}_i = \omega_i - \sum_j A_{ij} \sin(\varphi_i - \varphi_j + \delta_{ij}), \quad (32)$$

where δ_{ij} is an anti-symmetric matrix representing the phase differences we wish to code. The main problem with equation (32) is that it does not have a clear physical interpretation. How are arbitrary phases learned? Furthermore, since the A_{ij} represent oscillator couplings, how are the phase differences stored? To answer these questions, let us rewrite (32) as

$$\dot{\varphi}_i = \omega_i - \sum_j A_{ij} [\cos(\delta_{ij}) \sin(\varphi_i - \varphi_j) + \sin(\delta_{ij}) \cos(\varphi_i - \varphi_j)]. \quad (33)$$

Since the terms involving the phase differences δ_{ij} are constant, we can write (33) as

$$\dot{\varphi}_i = \omega_i - \sum_j [k_{ij}^E \sin(\varphi_i - \varphi_j) + k_{ij}^I \cos(\varphi_i - \varphi_j)],$$

where $k_{ij}^E = A_{ij} \cos(\delta_{ij})$ and $k_{ij}^I = A_{ij} \sin(\delta_{ij})$. Equation (32) has an immediate physical interpretation. Since k_{ij}^E makes oscillators φ_i and φ_j approach each other, we can think of them as corresponding to excitatory couplings between neurons or sets of neurons. When a neuron φ_j fires shortly before it is time for φ_i to fire, this makes it more probable φ_i will fire earlier, thus bringing its rate closer to φ_j . For k_{ij}^I the effect is the opposite: if a neuron in φ_j fires, k_{ij}^I makes the neurons in φ_i to fire further away from it. Therefore, k_{ij}^I represent inhibitory connections between φ_i and φ_j . In other words, to give physical meaning to learning phase differences in (32), we need to rewrite it to include excitatory and inhibitory terms.

Now that we have the basic tools, let us write the detailed model for three oscillators. We start with one stimulus oscillator, φ_s , and two response oscillators, φ_{r_1} and φ_{r_2} . The modified Kuramoto oscillators, with terms that allow for inhibitory connections,

are

$$\begin{aligned}\frac{d\varphi_s}{dt} = & \omega_0 - k_{s,r_1}^E \sin(\varphi_s - \varphi_{r_1}) - k_{s,r_2}^E \sin(\varphi_s - \varphi_{r_2}) \\ & - k_{s,r_1}^I \cos(\varphi_s - \varphi_{r_1}) - k_{s,r_2}^I \cos(\varphi_s - \varphi_{r_2}),\end{aligned}\quad (34)$$

$$\begin{aligned}\frac{d\varphi_{r_1}}{dt} = & \omega_0 - k_{r_1,s}^E \sin(\varphi_{r_1} - \varphi_s) - k_{r_1,r_2}^E \sin(\varphi_{r_1} - \varphi_{r_2}) \\ & - k_{r_1,s}^I \cos(\varphi_{r_1} - \varphi_s) - k_{r_1,r_2}^I \cos(\varphi_{r_1} - \varphi_{r_2}),\end{aligned}\quad (35)$$

$$\begin{aligned}\frac{d\varphi_{r_2}}{dt} = & \omega_0 - k_{r_2,s}^E \sin(\varphi_{r_2} - \varphi_s) - k_{r_2,r_1}^E \sin(\varphi_{r_2} - \varphi_{r_1}) \\ & - k_{r_2,s}^I \cos(\varphi_{r_2} - \varphi_s) - k_{r_2,r_1}^I \cos(\varphi_{r_2} - \varphi_{r_1}).\end{aligned}\quad (36)$$

Notice that in (34)–(36) the couplings are not necessarily symmetric. Though this is neurophysiologically reasonable, it is often the case that symmetric couplings are used in artificial neural network models.

For the yes-no oscillator model, (15)–(20) determined the changes to couplings associated to learning. Here, we alter (15)–(20) to include inhibitory neurons.

$$\begin{aligned}\frac{d\varphi_s}{dt} = & \omega_0 - k_{s,r_1}^E \sin(\varphi_s - \varphi_{r_1}) - k_{s,r_2}^E \sin(\varphi_s - \varphi_{r_2}) \\ & - k_{s,r_1}^I \cos(\varphi_s - \varphi_{r_1}) - k_{s,r_2}^I \cos(\varphi_s - \varphi_{r_2}) \\ & - K_0 \sin(\varphi_s - \omega_e t),\end{aligned}\quad (37)$$

$$\begin{aligned}\frac{d\varphi_{r_1}}{dt} = & \omega_0 - k_{r_1,s}^E \sin(\varphi_{r_1} - \varphi_s) - k_{r_1,r_2}^E \sin(\varphi_{r_1} - \varphi_{r_2}) \\ & - k_{r_1,s}^I \cos(\varphi_{r_1} - \varphi_s) - k_{r_1,r_2}^I \cos(\varphi_{r_1} - \varphi_{r_2}) \\ & - K_0 \sin(\varphi_{r_1} - \omega_e t - \delta\varphi),\end{aligned}\quad (38)$$

$$\begin{aligned}\frac{d\varphi_{r_2}}{dt} = & \omega_0 - k_{r_2,s}^E \sin(\varphi_{r_2} - \varphi_s) - k_{r_2,r_1}^E \sin(\varphi_{r_2} - \varphi_{r_1}) \\ & - k_{r_2,s}^I \cos(\varphi_{r_2} - \varphi_s) - k_{r_2,r_1}^I \cos(\varphi_{r_2} - \varphi_{r_1}) \\ & - K_0 \sin(\varphi_{r_2} - \omega_e t - \delta\varphi + \pi),\end{aligned}\quad (39)$$

where K_0 is the reinforcement constant, as before. For the excitatory couplings, we use the same learning equations as before, namely (18)–(20), as they reinforce the couplings when the oscillators are synchronizing. With the asymmetric form, we now have the following six sets of differential equations, where we use the same function

$\epsilon(K_0)$ as in (21).

$$\frac{dk_{s,r_1}^E}{dt} = \epsilon(K_0) [\alpha \cos(\varphi_s - \varphi_{r_1}) - k_{s,r_1}^E], \quad (40)$$

$$\frac{dk_{s,r_2}^E}{dt} = \epsilon(K_0) [\alpha \cos(\varphi_s - \varphi_{r_2}) - k_{s,r_2}^E], \quad (41)$$

$$\frac{dk_{r_1,r_2}^E}{dt} = \epsilon(K_0) [\alpha \cos(\varphi_{r_1} - \varphi_{r_2}) - k_{r_1,r_2}^E], \quad (42)$$

$$\frac{dk_{r_1,s}^E}{dt} = \epsilon(K_0) [\alpha \cos(\varphi_s - \varphi_{r_1}) - k_{r_1,s}^E], \quad (43)$$

$$\frac{dk_{r_2,s}^E}{dt} = \epsilon(K_0) [\alpha \cos(\varphi_s - \varphi_{r_2}) - k_{r_2,s}^E], \quad (44)$$

$$\frac{dk_{r_2,r_1}^E}{dt} = \epsilon(K_0) [\alpha \cos(\varphi_{r_1} - \varphi_{r_2}) - k_{r_2,r_1}^E]. \quad (45)$$

Similarly, for inhibitory connections, if two oscillators are perfectly off sync, then we have a reinforcement of the inhibitory connections. This is realized with the following set of six differential equations for the inhibitory couplings.

$$\frac{dk_{s,r_1}^I}{dt} = \epsilon(K_0) [\alpha \sin(\varphi_s - \varphi_{r_1}) - k_{s,r_1}^I], \quad (46)$$

$$\frac{dk_{s,r_2}^I}{dt} = \epsilon(K_0) [\alpha \sin(\varphi_s - \varphi_{r_2}) - k_{s,r_2}^I], \quad (47)$$

$$\frac{dk_{r_1,r_2}^I}{dt} = \epsilon(K_0) [\alpha \sin(\varphi_{r_1} - \varphi_{r_2}) - k_{r_1,r_2}^I], \quad (48)$$

$$\frac{dk_{r_1,s}^I}{dt} = \epsilon(K_0) [\alpha \sin(\varphi_{r_1} - \varphi_s) - k_{r_1,s}^I], \quad (49)$$

$$\frac{dk_{r_2,s}^I}{dt} = \epsilon(K_0) [\alpha \sin(\varphi_{r_2} - \varphi_s) - k_{r_2,s}^I], \quad (50)$$

$$\frac{dk_{r_2,r_1}^I}{dt} = \epsilon(K_0) [\alpha \sin(\varphi_{r_2} - \varphi_{r_1}) - k_{r_2,r_1}^I]. \quad (51)$$

Before we proceed, let us analyze the asymptotic behavior of those equations. From (40)–(51) and with the assumption that K_0 is very large, we have

$$\begin{aligned} \frac{d\varphi_s}{dt} &\approx -K_0 \sin(\varphi_s - \omega_e t), \\ \frac{d\varphi_{r_1}}{dt} &\approx -K_0 \sin(\varphi_{r_1} - \omega_e t - \delta\varphi), \\ \frac{d\varphi_{r_2}}{dt} &\approx -K_0 \sin(\varphi_{r_2} - \omega_e t - \delta\varphi + \pi), \end{aligned}$$

which of course leads to the fixed points $\varphi_s = \omega_e t$, $\varphi_{r_1} = \omega_e t + \delta\varphi$, $\varphi_{r_2} = \omega_e t + \delta\varphi - \pi$.

With this reinforcement, the excitatory couplings go to the following asymptotic values

$k_{s,r_1}^E = k_{r_1,s}^E = -k_{s,r_2}^E = -k_{r_2,s}^E = \alpha \cos(\delta\varphi)$, $k_{r_1,r_2}^E = k_{r_2,r_1}^E = -\alpha$, and the inhibitory go to $k_{s,r_1}^I = -k_{r_1,s}^I = -k_{s,r_2}^I = k_{r_2,s}^I = \alpha \sin(\delta\varphi)$, and $k_{r_1,r_2}^I = k_{r_2,r_1}^I = 0$. We show in Appendix B that these couplings lead to the desired fixed points.

Thus, a modification of Kuramoto's equations, where we include asymmetric couplings and inhibitory connections, permit the coding of any desired phase differences. Learning becomes more complex, as several new equations are necessary to accommodate the lack of symmetries. However, the underlying ideas are the same, i.e., that learning happens in a Hebb-like fashion, via the strengthening of inhibitory and excitatory oscillator couplings during reinforcement.

The coded phase differences may be used to model a continuum of responses within SR theory in the following way. At the beginning of the trial, the oscillators are reset with a small fluctuation, as in the one-element model, according to the distribution (7). Then, the system evolves according to (34)–(36) if no reinforcement is present, and according to (37)–(51) if a reinforcement is present. The probabilistic characteristics of the initial conditions lead to the smearing of the phase differences after a certain time, with an effect similar to the smearing distribution on the SR model for a continuum of responses (Suppes and Frankmann (1961); Suppes et al. (1964a)). We emphasize that the smearing distribution is not introduced as an extra feature of the oscillator model, but comes naturally from the stochastic properties of it.

4. Comparison with Experiment

Although the oscillator models produce a mean learning curve that fits quite well the one predicted by SR theory, it is well known that stochastic models with underlying assumptions that are qualitatively quite different may predict the same mean learning curves. The asymptotic conditional probabilities given by (2)–(5), on the other hand, have very different values, depending on the number N of sampled stimuli assumed. For instance, the observable conditional probability $P_\infty(R_{1,n+1}|E_{2,n}R_{2,n})$ is zero for the one-stimulus model and different from zero for the other models; nevertheless, given $c_1 = c_N/N$, the N -stimulus model and the one-stimulus model predict exactly the same mean learning curve, where c_1 is the conditioning parameter for the one-stimulus model and c_N is such for the N -stimulus model.

The lesson is that we often cannot distinguish two models by looking at their mean behavior, but the conditional probabilities of the N -stimulus model for N equals 1, 2, and 3 are quite different. In the following, we compare such theoretical quantities with two behavioral experiments and oscillator-model simulated data.

4.1. Experiment on paired-associate learning

In this experiment by Bower, analyzed in detail in (Bower, 1961), twenty-nine subjects learned a list of ten stimulus items to a criterion of two consecutive errorless cycles. The order of stimulus presentation was randomized for each trial. The stimuli were different pairs of consonant letters; the numerical responses were the numbers 1 and 2, each number being assigned as correct to a randomly selected five stimuli for each subject. The subject was informed of the correct answer following each response. The one-stimulus model fitted the behavioral data the best.

Here we used 29 independent sets of oscillators, each set with ten-stimulus, two-response, and two-reinforcement oscillators, to reproduce Bower's experimental setup. We stress that this is not equivalent to a ten-stimulus model, as each stimulus oscillator corresponds to a unique observable stimulus, since we have only two response oscillators with coupling k_{r_1, r_2} . For our simulations we set $N = 1$ and $K' = 94 \text{ s}^{-1}$. K' was chosen based on (25) and on Bower's statistical estimation of the probability of effective reinforcement for the one-stimulus model as $c = 0.344$.

Bower's behavioral data were also tested in Suppes and Ginsberg (1963) for the statistical properties of stationarity and independence prior to the last response error. We compare in Table 2 the behavioral results with those for our oscillator simulation.

Stationarity. The first test is that of stationarity, i.e., whether the probability of a response oscillator locking before the last error is constant. To perform this test, we restricted our data set to the M responses that happened *before* the last error for a given subject. We then divided this set into two, with the first $M/2$ trials being early trials and the remaining $M/2$ late trials. Let n_1 be the number of correct responses in the first half and n_2 the number of correct responses in the second half. If the probability is stationary, then both $n_1/(M/2)$ and $n_2/(M/2)$ should be approximately $(n_1 + n_2)/M$. We used a standard χ^2 test for this null hypothesis of stationarity.

Independence. Restricting ourselves again to trials prior to the last error, let n_{ij} be the number of transitions from state i to state j , where i and j can take values 0 (correct response) or 1 (incorrect). We use these numbers to estimate the transition probabilities p_{ij} . The null hypothesis of independence is that $p_{00} = p_{10}$ and $p_{01} = p_{11}$.

Table 2: Comparison between the paired-associate experimental data and the simulated one-stimulus oscillator model.

	Stationarity
Paired-associate	$\chi^2 = .97, N = 549,$ $df = 6, p > .95$
Oscillator model	$\chi^2 = 2.69, N = 748,$ $df = 1, p > .1$
	Independence
Paired-associate	$\chi^2 = .97, N = 549,$ $df = 6, p > .95$
Oscillator model	$\chi^2 = 0.1, N = 458,$ $df = 1, p > .75$

The sample paths used to compute the oscillator results in Table 2 were obtained by running simulations in MATLAB 7.1.0.183 (R14), SP 3 with the parameter values given earlier. The simulations consisted of randomly selecting, at each trial, the initial phase according to (7) and then computing phase evolution during Δt_r by numerically solving (8)–(10) using MATLAB’s built-in fourth-fifth order Runge-Kutta method. After Δt_r the phase differences were computed and a response oscillator selected. At the beginning of reinforcement, new initial conditions and a random value for K_0 were drawn according to (7) and (14), respectively. If $K_0 > K'$, then the oscillators’ couplings changed according to (15)–(20), and these equations were numerically solved for the time interval Δt_e also using fourth-fifth order Runge-Kutta, and the new values for the couplings were used on the next trial.

4.2. Experiment on probability matching

Another experiment that we modeled with oscillators is a probability-matching one, described in detail in (Suppes and Atkinson, 1960, Chapter 10). The experiment consisted of 30 subjects, who had to choose between two possible behavioral responses, R_1 or R_2 . A top light on a panel would turn on to indicate to the subject the beginning

of a trial. Reinforcement was indicated by a light going on over the correct response key. The correct response was noncontingent, with probability $\beta = 0.6$ for E_1 and 0.4 for E_2 . The experiment consisted of 240 trials for each subject.

To compare the oscillator model with the results for the probability-matching experiment, we first computed, using the behavioral data for the last 100 trials, the pseudomaximum likelihood function

$$L(c, N) = \sum_{i,j,k=1}^2 n_{ij,k} \log P_{\infty}(R_{k,n+1}|E_{j,n}R_{i,n}),$$

where $n_{ij,k}$ is the observed number of transitions from R_i and E_j on trial n to R_k on trial $n + 1$, and the conditional probabilities $P_{\infty}(R_{k,n+1}|E_{j,n}R_{i,n})$ are given by (2)–(5). The function $L(c, N)$, with $\beta = 0.6$ as in the experiment, had maxima at $\hat{c} = 0.568$ for $N = 2$, $\hat{c} = 0.600$ for $N = 3$, $\hat{c} = 0.631$ for $N = 4$, and $\hat{c} = 0.611$ for $\hat{N} = 3.35$, where \hat{N} is the pseudomaximum likelihood estimate of N (more details are shown in Appendix E). We ran MATLAB simulations, as described above, for 240 trials and 30 sets of oscillators, one for each subject, for the two, three, and four-stimulus oscillator models. We did not include here the one-stimulus model, already applied to Bower's experiment, because it predicts conditional probabilities that are grossly incorrect for the current experiment. Since the behavioral learning parameter c relates to K' , we used $K' = 73 \text{ s}^{-1}$, $K' = 65 \text{ s}^{-1}$, and $K' = 56 \text{ s}^{-1}$ for the two, three, and four-stimulus models, respectively, corresponding to $\hat{c} = 0.568$, $\hat{c} = 0.600$, and $\hat{c} = 0.631$. Table 3 compares the experimentally observed conditional relative frequencies, the predicted asymptotic values for the three different SR models, the best fitting \hat{N} -stimulus model, and simulations for oscillator models. In Table 3, $P(r_{1,n+1}|e_{1,n}r_{1,n})$ is the asymptotic conditional probability of response oscillator r_1 on trial $n + 1$ if on trial n the response oscillator was r_1 and the reinforcement oscillator was e_1 , and similarly for the other three expressions. The corresponding theoretical conditional probabilities predicted by the behavioral models are given by (2)–(5).

The results in Table 2 show that we cannot sharply differentiate the data from the null hypothesis of stationarity and independence. In Table 3 we compare the oscillator models to the behavioral data and the best fitting asymptotic SR models. Each oscillator model was computed using the same estimated c value as the corresponding SR model.

Table 3: Comparison between experimental results, SR models, and the corresponding oscillator models. For the N -stimulus model, we used $\hat{N} = 3.35$ and $\hat{c} = 0.611$, values that maximize $L(c, N)$. The first data column shows experimental values based on the last 100 trials of the 30-subject group. The other columns show the SR-theory asymptotic probabilities and simulations for the oscillator models averaged over the last 100 trials.

Asymptotic	Observed	2-el.	2-el. osc.	3-el.	3-el. osc.	\hat{N} -el.	4-el.	4-el. osc.
$P(r_1 e_1r_1)$.715	.800	.804	.733	.705	.719	.700	.760
$P(r_1 e_1r_2)$.602	.584	.569	.600	.574	.603	.608	.610
$P(r_1 e_2r_1)$.535	.516	.437	.533	.522	.537	.542	.538
$P(r_1 e_2r_2)$.413	.300	.309	.400	.381	.421	.450	.426

The fit of the $\hat{N} = 3.35$ SR model to the behavioral data is quite good, and that of the $N = 4$ SR model nearly as good. Moreover, the 4-stimulus oscillator fits very well with the $\hat{N} = 3.35$ stimulus SR model.

4.3. Continuum of Responses

One of the main changes to SR theory when dealing with a continuum of responses is the introduction of a smearing distribution $k(x; y)$ (for details, see (Suppes, 1959; Suppes and Frankmann, 1961)). Before we compare our oscillator model with the interesting case of a reinforcement given by a bimodal distribution, it is worth investigating the smearing distribution for our oscillator model. Let us consider a simple reinforcement $f(y)$ given by a Dirac delta function centered in a , $0 \leq a < 2\pi$, i.e. $f(y) = \delta(y - a)$. Then, according to (6), the response distribution $r(x)$ becomes asymptotically

$$r(x) = \int_0^{2\pi} k(x; y)\delta(y - a)dy = k(x; a),$$

i.e. $r(x)$ coincides with the smearing distribution at the point of reinforcement a . Thus, by using a reinforcement density given by a Dirac delta function at a , we are able to obtain the shape of the smearing distribution. Figure 3

shows the density histogram for a MATLAB simulation of the three oscillator model given in Section 3.2 using a Dirac function centered on $\pi/3$. The histogram was obtained using 6300 points corresponding to 300 oscillators and 21 reinforcement trials per set of oscillators (trials 40 to 60). All parameters used were the same as those for the one-element model, with some important exceptions. In the continuum of responses we need to have both inhibitory and excitatory connections. To accommodate

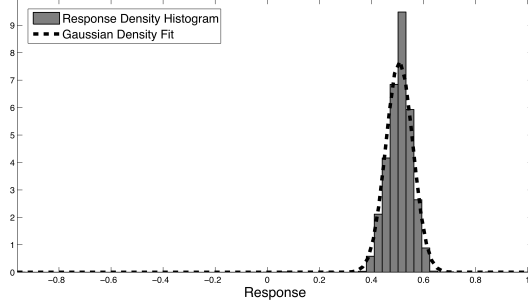


Figure 3: Histogram density of 300 oscillator models with a reinforcement angle of $\pi/3$ for the interval $(-\pi, \pi)$, which corresponds to $b = 0.5$ in (31). The fitted Gaussian has $\mu = 0.51$ and $\sigma = 0.05$, with $p < 10^{-3}$.

the effects of such connections, the driving learning term in (37)–(39) needs to be increased, and we changed K'_0 to 4,500, $\bar{K}_0 = 4,000$, and $\sigma_{K_0} = 1,000$. Also, to make the model more realistic, for each set of oscillators we randomly selected the oscillator frequencies with variance 1 around the mean 10 Hz, instead of setting all oscillators to the same frequency. We emphasize that the change in parameters is actually a requirement of the more complex model, and represents a further constraint in the parameters due to the extra complexity of the model. Figure 3 shows that the model's smearing distribution $f(x; y)$ is a Gaussian. We should mention that the estimation of the smearing distribution from a reinforcement schedule given by the Dirac delta function is not realistic for real psychological experiments. However, because we are running simulations without taking into consideration other behavioral and environmental aspects, we are able to extract $f(x; y)$ from our simulation data.

Let us now focus on the experiment described in Suppes et al. (1964b). In it, a screen had a 5-foot diameter circle. A non-contingent reinforcement was given on each trial by a red light on the 5-foot circle, with the position determined by a bimodal distribution $f(x)$, given by

$$f(x) = \begin{cases} \frac{2}{\pi^2}x, & 0 \leq x \leq \frac{\pi}{2} \\ \frac{2}{\pi^2}(\pi - x), & \frac{\pi}{2} < x \leq \pi \\ \frac{2}{\pi^2}(x - \pi), & \pi < x \leq \frac{3\pi}{2} \\ \frac{2}{\pi^2}(2\pi - x), & \frac{3\pi}{2} < x \leq 2\pi. \end{cases} \quad (52)$$

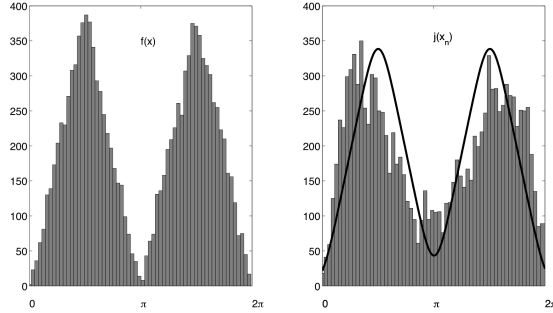


Figure 4: Histograms of reinforcement angles for the distribution $f(x)$ (left), and response density $j(x_n)$ (right). The black line shows the fitted SR theoretical predictions of the one-element model using the smearing distribution of Fig. 3.

At the center of this circle, a knob connected to an invisible shaft allowed a red light to be projected on the screen at any point on the 5-foot diameter circle. Subjects were instructed to use this knob to predict on each trial the position of the next reinforcement light. In Suppes et al. (1964b), subjects were 4 males and 26 female Stanford undergraduates. For this experiment, Suppes et al. (1964b) discuss many points related to the predictions of SR theory, including goodness of fit. Here we focus mainly on the relationship between our oscillator model and the smearing distribution $k(x; y)$, and on the conditional probability densities.

Our main results for the continuum of responses are in Figures 4–7, where we show the results of a 600-trial simulation for each of the 30 subjects. The histograms were computed using the last 400 trials, for a total of 12,000 sample points, and b was reparametrized to correspond to the interval $(0, 2\pi)$. In Figures 4–7, the parameters used are the same as above, with the exception of $K'_0 = 4468$, chosen such that the learning effectiveness of the oscillator model would coincide with the observed value of $c = 0.32$ in Suppes et al. (1964b). Figure

4 shows the effects of the smearing distributions on the responses. Figure

5 shows the conditional response density $j(x_n|Y_{n-1})$ if reinforcement on the previous trial $(n-1)$ happened on the interval $(\pi, 3\pi/2)$. As predicted by SR-theory, the oscillator model also exhibits an asymmetric distribution for the conditional density. We also compute the second order conditional distributions $j(x_n|Y_{n-1}Y_{n-2})$, shown in Figure

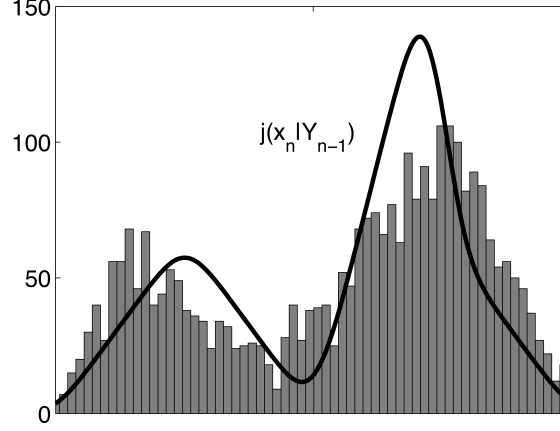


Figure 5: Histogram for the response x_n on trial n conditioned to a reinforcement on trial $n - 1$ in the interval $(\pi, 3\pi/2)$. The black line shows the fitted SR theoretical predictions of the one-element model using the smearing distribution of Fig. 3.

6. Finally, if we use our data to generate the conditional densities $j(x_n | Y_{n-1} X_{n-1})$, we obtain a similar result to that of the 1-element model (see Figure 7). We emphasize that, as in the N -element oscillator model used for the paired-associate learning experiment, the continuum-of-responses oscillator model can be modified to yield similar statistical predictions as the SR-model, if we add oscillators to represent additional elements.

5. Conclusions and Final Remarks

We represented SR models by neural oscillator models based on reasonable assumptions from neurophysiology. The effects of the interaction between the neural oscillators were described by phase differences obeying Kuramoto's equations. Learning was modeled by changes in phases and couplings driven by a reinforcement oscillator, with phase locking corresponding to behavioral conditioning. We compared the oscillator models to two behavioral experiments, as well as corresponding behavioral models derived from SR theory. Our simulation results support the claim that neural oscillators may be used to represent, in reasonable approximation, SR models.

From (25), behavioral and experimental data relate the SR conditioning parameter c to K' , σ_{K_0} , and \bar{K}_0 , but their range is not constrained by it. Despite the large

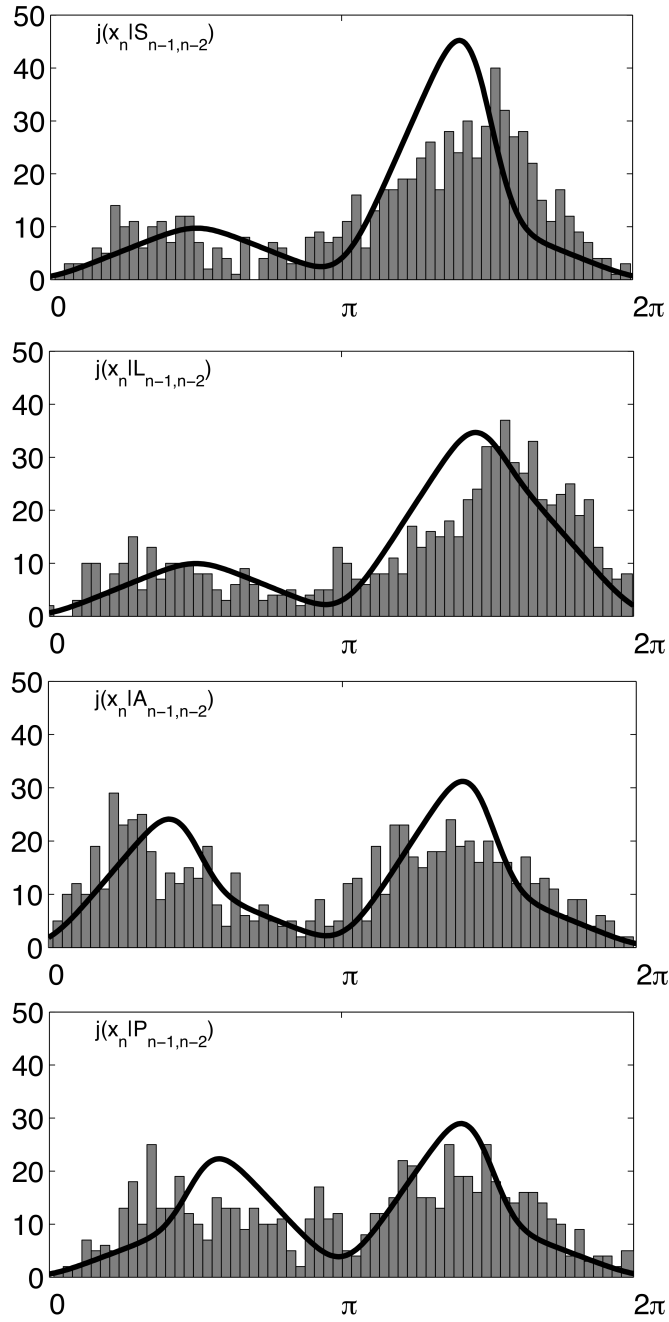


Figure 6: Simulated response histogram for the response conditioned to reinforcement on the two previous trials. All graphs correspond to responses with reinforcement on trial $n - 1$ being on the interval $(\pi, 3\pi/2)$. S corresponds to reinforcements on trial $n - 2$ both occurring on the same interval. L corresponds to reinforcement on $n - 2$ occurring on the interval $(3\pi/2, 2\pi)$, A on the interval $(0, \pi/2)$, and P on $(\pi/2, \pi)$. The solid lines show the SR theoretical one-element model predictions.

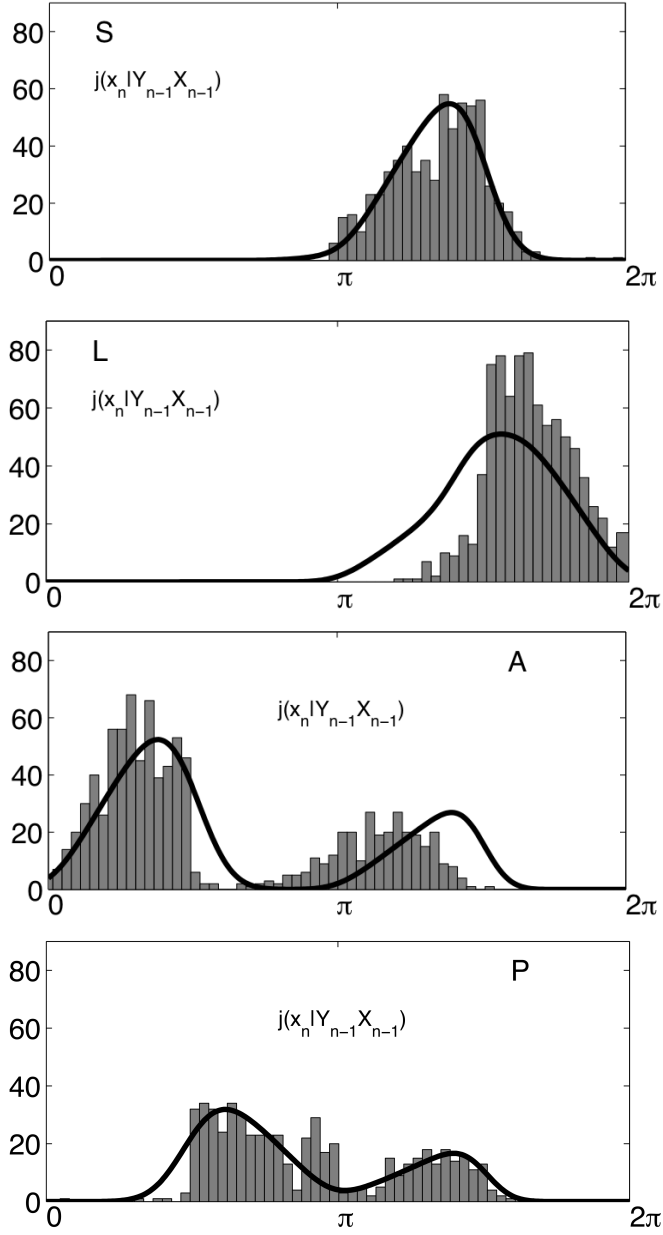


Figure 7: Simulated response histogram for the response conditioned to reinforcement and response on the previous trials. All graphs correspond to responses with reinforcement on trial $n - 1$ being on the interval $(\pi, 3\pi/2)$. S corresponds to responses on trial $n - 1$ occurring on the same interval. L corresponds to responses on $n - 1$ occurring on the interval $(3\pi/2, 2\pi)$, A on the interval $(0, \pi/2)$, and P on $(\pi/2, \pi)$. The solid lines are the SR predictions from the one-element model.

number of parameters, our numerical simulations, all done with the same set of parameters, except N and K' , show that the statistical fit reported in Table 2 and conditional probabilities in Table 3 do not vary much even when these parameters are changed significantly. The most important constraint is this. Once all parameters are fixed then the SR conditioning parameter c is a nonlinear monotonically decreasing function of K' given by (25). As our oscillators are refined and extended to more experiments, further constraints should narrow the parameter space.

As is sometimes remarked, SR theory abstracts from many necessary processes that must have a physical realization. From a general psychological viewpoint, independent of the details of physical realization, undoubtedly the most obvious missing process is the perceptual recognition of the sampling of the same, or nearly the same, physical stimulus pattern on repeated trials. We should be able to expand the present setup to include oscillators that recognize, by similarity or congruence computations, when a sampled stimulus type is one that has been previously sampled. Prior work on pattern recognition will be useful here. Our own earlier experimental work on computational models that recognize auditory or visual word, sentence or other brain images, such as those of red triangles or blue circles, provides substantial evidence that a single oscillator with one given natural frequency will be inadequate. Multiple oscillators with different natural frequencies will be required for such similarity recognition. For examples of such computational models applied to EEG-recorded brain data, see Suppes et al. (1997, 1998, 1999b,a) for Fourier methods, de Barros et al. (2006) for a Laplacian model, and Wong et al. (2006) for perceptron models with regularization and independent component analysis.

The oscillator models developed provide a schematic model of psychological processes successfully modeled behaviorally using stimulus-response theory. The weakly coupled neural phase oscillators used offer a physical mechanism to explain schematically how conditioning works in the brain. Many important physical details of such processes remain to be clarified by future work. But, in the mean time, as psychology and system neuroscience draw closer together, it is desirable that specific, even if only schematic, physical mechanisms be proposed to provide conceptually plausible physical realizations of fundamental psychological processes. The most important

idea tested here is that the main physical mechanism in SR learning is phase-locking, a concept widely used in physics, but not in psychology, or, even as yet, much in system neuroscience.

Appendix A. Appendix - Stability of Fixed Points

In this appendix we derive the stability conditions for the fixed points of equations

$$\begin{aligned} \frac{d\varphi_{s_j}}{dt} &= \omega_0 - k_{s_j,r_1} \sin(\varphi_{s_j} - \varphi_{r_1}) \\ &\quad - k_{s_j,r_2} \sin(\varphi_{s_j} - \varphi_{r_2}), \end{aligned} \quad (\text{Appendix A.1})$$

$$\begin{aligned} \frac{d\varphi_{r_1}}{dt} &= \omega_0 - k_{s_j,r_1} \sin(\varphi_{r_1} - \varphi_{s_j}) \\ &\quad - k_{r_1,r_2} \sin(\varphi_{r_1} - \varphi_{r_2}), \end{aligned} \quad (\text{Appendix A.2})$$

$$\begin{aligned} \frac{d\varphi_{r_2}}{dt} &= \omega_0 - k_{s_j,r_2} \sin(\varphi_{r_2} - \varphi_{s_j}) \\ &\quad - k_{r_1,r_2} \sin(\varphi_{r_2} - \varphi_{r_1}), \end{aligned} \quad (\text{Appendix A.3})$$

in the case of three coupled oscillators, s_j , r_1 , and r_2 . Since we are mainly interested in phase differences, we define $\phi_{1s} = \varphi_{r_1} - \varphi_{s_j}$ and $\phi_{2s} = \varphi_{r_1} - \varphi_{s_j}$, and substitute them in (Appendix A.1)–(Appendix A.1). Then, (Appendix A.1)–(Appendix A.1) reduce to the following pair of coupled differential equations.

$$\begin{aligned} \frac{d\phi_{1s}}{dt} &= -2k_{s,r_1} \sin(\phi_{1s}) - k_{s,r_2} \sin(\phi_{2s}) \\ &\quad - k_{r_1,r_2} \sin(\phi_{1s} - \phi_{2s}), \end{aligned} \quad (\text{Appendix A.4})$$

$$\begin{aligned} \frac{d\phi_{2s}}{dt} &= -k_{s,r_1} \sin(\phi_{1s}) - 2k_{s,r_2} \sin(\phi_{2s}) \\ &\quad + k_{r_1,r_2} \sin(\phi_{1s} - \phi_{2s}). \end{aligned} \quad (\text{Appendix A.5})$$

The question we want to answer is the following. Are there stable solutions to (Appendix A.4) and (Appendix A.5)? If so, how do they depend on the couplings?

To answer the above questions, we should first compute whether there are any fixed points for differential equations (Appendix A.4) and (Appendix A.5). Since a fixed point is a point where the system remains if initially placed on it, they are characterized by having both time derivatives of ϕ_{1j} and ϕ_{2j} equal to zero. Thus, the fixed points are

given by

$$-2k_{s,r_1} \sin(\phi_{1s}) - k_{s,r_2} \sin(\phi_{2s}) \quad (\text{Appendix A.6})$$

$$-k_{r_1,r_2} \sin(\phi_{1s} - \phi_{2s}) = 0,$$

$$-k_{s,r_1} \sin(\phi_{1s}) - 2k_{s,r_2} \sin(\phi_{2s}) \quad (\text{Appendix A.7})$$

$$+k_{r_1,r_2} \sin(\phi_{1s} - \phi_{2s}) = 0.$$

Because of the periodicity of the sin function, there are infinitely many fixed points. Since we are interested in phases, we don't need to examine all points, but it suffices to focus on the region determined by $0 \leq \phi_{1s} < 2\pi$ and $0 \leq \phi_{2s} < 2\pi$. The trivial fixed points, corresponding to each sin function in (Appendix A.6) and (Appendix A.7) being zero, are $(0, 0)$, $(\pi, 0)$, $(0, \pi)$, and (π, π) . The other solutions to (Appendix A.6) and (Appendix A.7) depend on the values of the coupling constants. To simplify our analysis, let us consider the case where all couplings have the same intensity, i.e. $|k_{s,r_1}| = |k_{r_1,r_2}| = |k_{s,r_2}|$. Since mainly the relative coupling strengths are relevant for matters of stability, let us consider the following scenarios: $k \equiv k_{s,r_1} = k_{s,r_2} = k_{r_1,r_2}$, $k \equiv -k_{s,r_1} = k_{s,r_2} = k_{r_1,r_2}$, $k \equiv k_{s,r_1} = -k_{s,r_2} = k_{r_1,r_2}$, and $k \equiv k_{s,r_1} = k_{s,r_2} = -k_{r_1,r_2}$. Other cases, like $-k_{s,r_1} = -k_{s,r_2} = k_{r_1,r_2}$, are contained on those, since k can be either positive or negative. Let us examine each case separately.

Appendix A.1. $k \equiv k_{s,r_1} = k_{s,r_2} = k_{r_1,r_2}$

For this case, in addition to $\{(0, 0), (0, \pi), (\pi, 0), (\pi, \pi)\}$, we have $(\frac{2}{3}\pi, -\frac{2}{3}\pi)$ and $(-\frac{2}{3}\pi, \frac{2}{3}\pi)$ as fixed points. Let us start with $\{(0, 0), (0, \pi), (\pi, 0), (\pi, \pi)\}$. In order to analyze their local stability, we linearize Kuramoto's equations (Appendix A.4) and (Appendix A.5) around $\{(0, 0), (0, \pi), (\pi, 0), (\pi, \pi)\}$. To linearize the equations, first we substitute ϕ_{1s} and ϕ_{2s} by $a + \epsilon_1$ and $b + \epsilon_2$, where a and b are the coordinates of the fixed points. Then we make a linear approximation for the sin function for values close to the fixed point, i.e. for ϵ_1 and ϵ_2 being small.

For example, for $(0, \pi)$ we define $\phi_{1s} = \epsilon_1$ and $\phi_{2s} = \pi + \epsilon_2$. Then (Appendix A.4)

and (Appendix A.5) become

$$\begin{aligned} \frac{d\epsilon_1}{dt} &= -2k_{s,r_1} \sin(\epsilon_1) - k_{s,r_2} \sin(\pi + \epsilon_2) & (\text{Appendix A.8}) \\ &\quad - k_{r_1,r_2} \sin(\epsilon_1 - \epsilon_2 - \pi), \end{aligned}$$

$$\begin{aligned} \frac{d\epsilon_2}{dt} &= -k_{s,r_1} \sin(\epsilon_1) - 2k_{s,r_2} \sin(\pi + \epsilon_2) & (\text{Appendix A.9}) \\ &\quad + k_{r_1,r_2} \sin(\epsilon_1 - \epsilon_2 - \pi). \end{aligned}$$

Because close to the fixed points $\epsilon_1 \ll 1$ and $\epsilon_2 \ll 1$, we make the approximation that $\sin(\epsilon_1) \approx \epsilon_1$ and $\sin(\epsilon_2) \approx \epsilon_2$, and (Appendix A.8) and (Appendix A.9) can be written as

$$\frac{d\epsilon_1}{dt} = -2k_{s,r_1} \epsilon_1 + k_{s,r_2} \epsilon_2 + k_{r_1,r_2} (\epsilon_1 - \epsilon_2), \quad (\text{Appendix A.10})$$

$$\frac{d\epsilon_2}{dt} = -k_{s,r_1} \epsilon_1 + 2k_{s,r_2} \epsilon_2 - k_{r_1,r_2} (\epsilon_1 - \epsilon_2), \quad (\text{Appendix A.11})$$

or

$$\frac{d\epsilon_1}{dt} = -k_{s,r_1} \epsilon_1, \quad (\text{Appendix A.12})$$

$$\frac{d\epsilon_2}{dt} = -2k_{s,r_1} \epsilon_1 - 3k_{s,r_2} \epsilon_2. \quad (\text{Appendix A.13})$$

The eigenvalues for the linearized (Appendix A.12) and (Appendix A.13) are $-k$ and $3k$. A fixed point is Liapunov stable if its eigenvalues are negative (Guckenheimer and Holmes, 1983). Therefore, for $k \equiv k_{s,r_1} = k_{s,r_2} = k_{r_1,r_2}$, the fixed point $(0, \pi)$ cannot be stable.

We perform the same computations for the other fixed points. The linearized equations are

$$\frac{d\epsilon_1}{dt} = -3k\epsilon_1, \quad (\text{Appendix A.14})$$

$$\frac{d\epsilon_2}{dt} = -3k\epsilon_2, \quad (\text{Appendix A.15})$$

for $(0, 0)$,

$$\frac{d\epsilon_1}{dt} = -k\epsilon_1, \quad (\text{Appendix A.16})$$

$$\frac{d\epsilon_2}{dt} = -2k\epsilon_1 + 3k\epsilon_2, \quad (\text{Appendix A.17})$$

once again, for $(0, \pi)$,

$$\frac{d\epsilon_1}{dt} = 3k\epsilon_1 - 2k\epsilon_2, \quad (\text{Appendix A.18})$$

$$\frac{d\epsilon_2}{dt} = -k\epsilon_2, \quad (\text{Appendix A.19})$$

for $(\pi, 0)$, and

$$\frac{d\epsilon_1}{dt} = k\epsilon_1 + 2k\epsilon_2, \quad (\text{Appendix A.20})$$

$$\frac{d\epsilon_2}{dt} = 2k\epsilon_1 + k\epsilon_2, \quad (\text{Appendix A.21})$$

for (π, π) . Only (Appendix A.14) and (Appendix A.15) have negative eigenvalues, if $k > 0$, thus correspond to fixed points that can be stable.

Now let us examine fixed points $(\frac{2}{3}\pi, -\frac{2}{3}\pi)$ and $(-\frac{2}{3}\pi, \frac{2}{3}\pi)$. Substituting $\phi_{1s} = \pm\frac{2}{3}\pi + \epsilon_1(t)$ and $\phi_{2s} = \mp\frac{2}{3}\pi + \epsilon_2(t)$ in (Appendix A.4) and (Appendix A.5), we have

$$\begin{aligned} \frac{1}{k} \frac{d\epsilon_1}{dt} &= -2 \sin\left(\pm\frac{2}{3}\pi + \epsilon_1\right) - \sin\left(\mp\frac{2}{3}\pi + \epsilon_2\right) \\ &\quad - \sin\left(\pm\frac{2}{3}\pi + \epsilon_1(t) \pm \frac{2}{3}\pi - \epsilon_2\right), \end{aligned} \quad (\text{Appendix A.22})$$

$$\begin{aligned} \frac{1}{k} \frac{d\epsilon_2}{dt} &= -\sin\left(\pm\frac{2}{3}\pi + \epsilon_1\right) - 2 \sin\left(\mp\frac{2}{3}\pi + \epsilon_2\right) \\ &\quad + \sin\left(\pm\frac{2}{3}\pi + \epsilon_1(t) \pm \frac{2}{3}\pi - \epsilon_2\right). \end{aligned} \quad (\text{Appendix A.23})$$

Using the linear approximation for $\epsilon_1 \ll 1$ and $\epsilon_2 \ll 1$ we get

$$\begin{aligned} \frac{1}{k} \frac{d\epsilon_1}{dt} &= -2 \left[\pm \sin\left(\frac{2}{3}\pi\right) + \cos\left(\frac{2}{3}\pi\right) \epsilon_1 \right] \\ &\quad - \left[\mp \sin\left(\frac{2}{3}\pi\right) + \cos\left(\frac{2}{3}\pi\right) \epsilon_2 \right] \\ &\quad - \left[\pm \sin\left(\frac{4}{3}\pi\right) + \cos\left(\frac{4}{3}\pi\right) (\epsilon_1 - \epsilon_2) \right], \end{aligned} \quad (\text{Appendix A.24})$$

$$\begin{aligned} \frac{1}{k} \frac{d\epsilon_2}{dt} &= - \left[\pm \sin\left(\frac{2}{3}\pi\right) + \cos\left(\frac{2}{3}\pi\right) \epsilon_1 \right] \\ &\quad - 2 \left[\mp \sin\left(\frac{2}{3}\pi\right) + \cos\left(\frac{2}{3}\pi\right) \epsilon_2 \right] \\ &\quad + \left[\pm \sin\left(\frac{4}{3}\pi\right) + \cos\left(\frac{4}{3}\pi\right) (\epsilon_1 - \epsilon_2) \right]. \end{aligned} \quad (\text{Appendix A.25})$$

or

$$\frac{1}{k} \frac{d\epsilon_1}{dt} = \frac{3}{2} \epsilon_1, \quad (\text{Appendix A.26})$$

$$\frac{1}{k} \frac{d\epsilon_2}{dt} = \frac{3}{2} \epsilon_2. \quad (\text{Appendix A.27})$$

This point is stable if $k < 0$. Thus, for $k \equiv k_{s,r_1} = k_{s,r_2} = k_{r_1,r_2}$, there are three stable fixed points: $(0, 0)$, $(\frac{2}{3}\pi, -\frac{2}{3}\pi)$, and $(-\frac{2}{3}\pi, \frac{2}{3}\pi)$. However, if $k > 0$ the only fixed point that is stable is $(0, 0)$, corresponding to the situation when all oscillators are exactly in phase.

Appendix A.2. $k \equiv -k_{s,r_1} = k_{s,r_2} = k_{r_1,r_2}$

Now the fixed points are $\{(0, 0), (0, \pi), (\pi, 0), (\pi, \pi), (\frac{2}{3}\pi, \frac{1}{3}\pi), (-\frac{2}{3}\pi, -\frac{1}{3}\pi)\}$. The linearized equations are

$$\frac{d\epsilon_1}{dt} = k\epsilon_1, \quad (\text{Appendix A.28})$$

$$\frac{d\epsilon_2}{dt} = 2k\epsilon_1 - 3k\epsilon_2, \quad (\text{Appendix A.29})$$

for $(0, 0)$,

$$\frac{d\epsilon_1}{dt} = 3k\epsilon_1, \quad (\text{Appendix A.30})$$

$$\frac{d\epsilon_2}{dt} = 3k\epsilon_2, \quad (\text{Appendix A.31})$$

for $(0, \pi)$,

$$\frac{d\epsilon_1}{dt} = -k\epsilon_1 - 2k\epsilon_2, \quad (\text{Appendix A.32})$$

$$\frac{d\epsilon_2}{dt} = -2k\epsilon_1 - k\epsilon_2, \quad (\text{Appendix A.33})$$

for $(\pi, 0)$, and

$$\frac{d\epsilon_1}{dt} = -3k\epsilon_1 + 2k\epsilon_2, \quad (\text{Appendix A.34})$$

$$\frac{d\epsilon_2}{dt} = k\epsilon_2, \quad (\text{Appendix A.35})$$

for (π, π) . Only (Appendix A.30) and (Appendix A.31) correspond to fixed points that can be stable, if $k < 0$, as there are no other choices of k that would allow the other points to be stable.

For fixed points $(\frac{2}{3}\pi, \frac{1}{3}\pi)$ and $(-\frac{2}{3}\pi, -\frac{1}{3}\pi)$, we substitute $\phi_{1s} = \pm\frac{2}{3}\pi + \epsilon_1(t)$ and $\phi_{2s} = \pm\frac{1}{3}\pi + \epsilon_2(t)$ in (Appendix A.4) and (Appendix A.5), and we have

$$\begin{aligned} \frac{d\epsilon_1}{dt} &= 2k \sin\left(\pm\frac{2}{3}\pi + \epsilon_1\right) - k \sin\left(\pm\frac{1}{3}\pi + \epsilon_2\right) \\ &\quad - k \sin\left(\pm\frac{2}{3}\pi \mp \frac{1}{3}\pi + \epsilon_1 - \epsilon_2\right), \end{aligned} \quad (\text{Appendix A.36})$$

$$\begin{aligned} \frac{d\epsilon_2}{dt} &= k \sin\left(\pm\frac{2}{3}\pi + \epsilon_1\right) - 2k \sin\left(\pm\frac{1}{3}\pi + \epsilon_2\right) \\ &\quad + k \sin\left(\pm\frac{2}{3}\pi \mp \frac{1}{3}\pi + \epsilon_1 - \epsilon_2\right). \end{aligned} \quad (\text{Appendix A.37})$$

Using the linear approximation for $\epsilon_1 \ll 1$ and $\epsilon_2 \ll 1$ we get

$$\frac{1}{k} \frac{d\epsilon_1}{dt} = -\frac{3}{2}\epsilon_1, \quad (\text{Appendix A.38})$$

$$\frac{1}{k} \frac{d\epsilon_2}{dt} = -\frac{3}{2}\epsilon_2. \quad (\text{Appendix A.39})$$

Points $(\frac{2}{3}\pi, \frac{1}{3}\pi)$ and $(-\frac{2}{3}\pi, -\frac{1}{3}\pi)$ are stable if $k > 0$. Thus, for $k \equiv -k_{s,r_1} = k_{s,r_2} = k_{r_1,r_2}$, there are three relevant stable fixed points: $(0, \pi)$, $(\frac{2}{3}\pi, \frac{1}{3}\pi)$ and $(-\frac{2}{3}\pi, -\frac{1}{3}\pi)$. However, if $k < 0$ the only fixed point that is stable is $(0, \pi)$, corresponding to the situation when the oscillators s and r_1 are in phase and s and r_2 are off phase by π .

Appendix A.3. $k \equiv k_{s,r_1} = -k_{s,r_2} = k_{r_1,r_2}$

For the points $\{(0, 0), (0, \pi), (\pi, 0), (\pi, \pi)\}$ the linearized form of (Appendix A.38) and (Appendix A.39) around the stability points are

$$\frac{d\epsilon_1}{dt} = -3k\epsilon_1 + 2k\epsilon_2, \quad (\text{Appendix A.40})$$

$$\frac{d\epsilon_2}{dt} = k\epsilon_2, \quad (\text{Appendix A.41})$$

for $(0, 0)$,

$$\frac{d\epsilon_1}{dt} = -k\epsilon_1 - 2k\epsilon_2, \quad (\text{Appendix A.42})$$

$$\frac{d\epsilon_2}{dt} = -2k\epsilon_1 - k\epsilon_2, \quad (\text{Appendix A.43})$$

for $(0, \pi)$,

$$\frac{d\epsilon_1}{dt} = 3k\epsilon_1, \quad (\text{Appendix A.44})$$

$$\frac{d\epsilon_2}{dt} = 3k\epsilon_2, \quad (\text{Appendix A.45})$$

for $(\pi, 0)$, and

$$\frac{d\epsilon_1}{dt} = k\epsilon_1, \quad (\text{Appendix A.46})$$

$$\frac{d\epsilon_2}{dt} = 2k\epsilon_1 - 3k\epsilon_2, \quad (\text{Appendix A.47})$$

for (π, π) . Only (Appendix A.44) and (Appendix A.45) correspond to fixed points that can be stable, if we choose $k < 0$. There are no choices of k that would allow the other points to be stable.

The other stable points are $(\frac{1}{3}\pi, \frac{2}{3}\pi)$ and $(-\frac{1}{3}\pi, -\frac{2}{3}\pi)$. The linearized (Appendix A.4) and (Appendix A.5) become

$$\begin{aligned} \frac{1}{k} \frac{d\epsilon_1}{dt} &= -2 \sin\left(\pm \frac{1}{3}\pi + \epsilon_1\right) + \sin\left(\pm \frac{2}{3}\pi + \epsilon_2\right) \\ &\quad - \sin\left(\pm \frac{1}{3}\pi + \epsilon_1 \mp \frac{2}{3}\pi - \epsilon_2\right), \end{aligned} \quad (\text{Appendix A.48})$$

$$\begin{aligned} \frac{1}{k} \frac{d\epsilon_2}{dt} &= -\sin\left(\pm \frac{1}{3}\pi + \epsilon_1\right) + 2 \sin\left(\pm \frac{2}{3}\pi + \epsilon_2\right) \\ &\quad + \sin\left(\pm \frac{1}{3}\pi + \epsilon_1 \mp \frac{2}{3}\pi - \epsilon_2\right). \end{aligned} \quad (\text{Appendix A.49})$$

Using the linear approximation for $\epsilon_1 \ll 1$ and $\epsilon_2 \ll 1$ we get

$$\begin{aligned} \frac{1}{k} \frac{d\epsilon_1}{dt} &= -\frac{3}{2}\epsilon_1, \\ \frac{1}{k} \frac{d\epsilon_2}{dt} &= -\frac{3}{2}\epsilon_2. \end{aligned}$$

This point is stable if $k > 0$. Thus, for $k \equiv k_{s,r_1} = -k_{s,r_2} = k_{r_1,r_2}$ there are three relevant stable fixed points: $(\pi, 0)$, $(\frac{1}{3}\pi, \frac{2}{3}\pi)$, and $(-\frac{1}{3}\pi, -\frac{2}{3}\pi)$, but if $k < 0$ only the point $(\pi, 0)$ is stable, corresponding to oscillator r_2 in phase with oscillator s , and r_1 off phase with s .

Appendix A.4. $k \equiv k_{s,r_1} = k_{s,r_2} = -k_{r_1,r_2}$

For the points $\{(0, 0), (0, \pi), (\pi, 0), (\pi, \pi)\}$, linearizing (Appendix A.38) and (Appendix A.39) gives us

$$\frac{d\epsilon_1}{dt} = -3k\epsilon_1, \quad (\text{Appendix A.50})$$

$$\frac{d\epsilon_2}{dt} = k\epsilon_2, \quad (\text{Appendix A.51})$$

for $(0, 0)$,

$$\frac{d\epsilon_1}{dt} = -3k\epsilon_1 + 2k\epsilon_2, \quad (\text{Appendix A.52})$$

$$\frac{d\epsilon_2}{dt} = k\epsilon_2, \quad (\text{Appendix A.53})$$

for $(0, \pi)$,

$$\frac{d\epsilon_1}{dt} = k\epsilon_1, \quad (\text{Appendix A.54})$$

$$\frac{d\epsilon_2}{dt} = 2k\epsilon_1 - 3k\epsilon_2, \quad (\text{Appendix A.55})$$

for $(\pi, 0)$, and

$$\frac{d\epsilon_1}{dt} = 3k\epsilon_1, \quad (\text{Appendix A.56})$$

$$\frac{d\epsilon_2}{dt} = 3k\epsilon_2, \quad (\text{Appendix A.57})$$

for (π, π) . Once again, only (Appendix A.56) and (Appendix A.57) correspond to fixed points that can be stable, if we choose $k < 0$.

The other fixed points are $(-\frac{1}{3}\pi, \frac{1}{3}\pi)$ and $(\frac{1}{3}\pi, -\frac{1}{3}\pi)$. Substituting $\phi_{1s} = \mp\frac{1}{3}\pi + \epsilon_1(t)$ and $\phi_{2s} = \pm\frac{1}{3}\pi + \epsilon_2(t)$ in (Appendix A.4) and (Appendix A.5), after a linear approximation for $\epsilon_1 \ll 1$ and $\epsilon_2 \ll 1$, we obtain

$$\frac{1}{k} \frac{d\epsilon_1}{dt} = -\frac{3}{2}\epsilon_1, \quad (\text{Appendix A.58})$$

$$\frac{1}{k} \frac{d\epsilon_2}{dt} = -\frac{3}{2}\epsilon_2. \quad (\text{Appendix A.59})$$

This point is stable if $k > 0$. For $k \equiv k_{s,r_1} = k_{s,r_2} = -k_{r_1,r_2}$ there are three relevant stable fixed points: (π, π) , $(\frac{2}{3}\pi, -\frac{2}{3}\pi)$, and $(-\frac{2}{3}\pi, \frac{2}{3}\pi)$.¹ However, if $k < 0$ the only fixed point that is stable is (π, π) , corresponding to the situation when both oscillators r_1 and r_2 are off phase with respect to oscillator s by π .

The results of Sections Appendix A.1–Appendix A.4 are summarized in Table A.4. If $k_{s,r_1} < 0$, the relative signs of the other coupling constants determine unique stability

¹In fact we have, as discussed above, an infinite number of stable fixed points. But since we are only interested in phase differences, and the fixed points other than $(\frac{2}{3}\pi, -\frac{2}{3}\pi)$ and $(-\frac{2}{3}\pi, \frac{2}{3}\pi)$ are periodic, with periodicity 2π , we omit them from our discussion.

	$k_{s,r_1} > 0$	$k_{s,r_1} < 0$
$k_{s,r_1} = k_{s,r_2} = k_{r_1,r_2}$	$(0, 0)$	$(\frac{2}{3}\pi, -\frac{2}{3}\pi)$ $(-\frac{2}{3}\pi, \frac{2}{3}\pi)$
$-k_{s,r_1} = k_{s,r_2} = k_{r_1,r_2}$	$(\frac{2}{3}\pi, \frac{1}{3}\pi)$ $(-\frac{2}{3}\pi, -\frac{1}{3}\pi)$	$(0, \pi)$
$k_{s,r_1} = -k_{s,r_2} = k_{r_1,r_2}$	$(\frac{1}{3}\pi, \frac{2}{3}\pi)$ $(-\frac{1}{3}\pi, -\frac{2}{3}\pi)$	$(\pi, 0)$
$k_{s,r_1} = k_{s,r_2} = -k_{r_1,r_2}$	$(-\frac{1}{3}\pi, \frac{1}{3}\pi)$ $(\frac{1}{3}\pi, -\frac{1}{3}\pi)$	(π, π)

Table A.4: Stable fixed points for $|k_{s,r_1}| = |k_{s,r_2}| = |k_{r_1,r_2}|$. Since the absolute values of the coupling strengths are all the same, which fixed points are stable is determined by the relative signs of the couplings.

points, corresponding to oscillator r_1 in phase with oscillator s and r_2 off phase by π (row 2), r_2 in phase and r_2 off phase by π (row 3), and both r_1 and r_2 off phase by π (row 4). The only possibility for all oscillators r_1 , r_2 , and s to be in phase is when all couplings are positive.

Appendix B. Appendix - Synchronization of oscillators

We are interested in knowing the qualitative behavior of the phases when a reinforcement occurs. During reinforcement, the oscillators satisfy equations

$$\begin{aligned} \frac{d\varphi_s}{dt} &= \omega_0 - k_{s,r_1} \sin(\varphi_s - \varphi_{r_1}) - k_{s,r_2} \sin(\varphi_s - \varphi_{r_2}) \\ &\quad + K_0 \sin(\varphi_s - \omega_e t), \end{aligned} \quad (\text{Appendix B.1})$$

$$\begin{aligned} \frac{d\varphi_{r_1}}{dt} &= \omega_0 - k_{s,r_1} \sin(\varphi_{r_1} - \varphi_s) - k_{r_1,r_2} \sin(\varphi_{r_1} - \varphi_{r_2}) \\ &\quad + K_0 \sin(\varphi_{r_1} - \omega_e t - \pi(1 - \delta_{e_n,1})), \end{aligned} \quad (\text{Appendix B.2})$$

$$\begin{aligned} \frac{d\varphi_{r_2}}{dt} &= \omega_0 - k_{s,r_2} \sin(\varphi_{r_2} - \varphi_s) - k_{r_1,r_2} \sin(\varphi_{r_2} - \varphi_{r_1}) \\ &\quad + K_0 \sin(\varphi_{r_2} - \omega_e t - \pi(1 - \delta_{e_n,2})), \end{aligned} \quad (\text{Appendix B.3})$$

$$\frac{dk_{s,r_1}}{dt} = \epsilon(K_0) [\alpha \cos(\varphi_s - \varphi_{r_1}) - k_{s,r_1}], \quad (\text{Appendix B.4})$$

$$\frac{dk_{s,r_2}}{dt} = \epsilon(K_0) [\alpha \cos(\varphi_s - \varphi_{r_2}) - k_{s,r_2}], \quad (\text{Appendix B.5})$$

$$\frac{dk_{r_1,r_2}}{dt} = \epsilon(K_0) [\alpha \cos(\varphi_{r_1} - \varphi_{r_2}) - k_{r_1,r_2}]. \quad (\text{Appendix B.6})$$

We show here that the first three equations lead the oscillators s , r_1 , and r_2 to synchronize and phase lock with reinforcement oscillators e_1 and e_2 if K_0 is sufficiently large.

We start with the approximation

$$\dot{\varphi}_s \approx \omega_0 + K_0 \sin(\varphi_s - \omega_e t),$$

for $K_0 \gg k_{r_1, r_2}, k_{s, r_1}, k_{s, r_2}$. An exact solution to this equation can be found, namely

$$\varphi_s = \omega_e t + 2 \arctan\left(-\frac{\Gamma}{\delta_{e0}}\right),$$

where $\Gamma = K_0 - \sqrt{\delta_{e0}^2 - K_0^2} \tan\left(\frac{1}{2}(t + c_1) \sqrt{\delta_{e0}^2 - K_0^2}\right)$, $\delta_{e0} = \omega_0 - \omega_e$, c_1 is an integration constant, and we assumed $\omega_e \neq \omega_0$. This equation shows a term with frequency ω_e plus another term that depends on t in a more complicated way. Let us assume, as we did in our article, that K_0 is large enough, such that $K_0 > |\omega_0 - \omega_e|$. This implies that the term inside the square root in the above equation is negative. Let

$$K_1 = i \sqrt{K_0^2 - \delta_{e0}^2} = i\kappa,$$

and we have

$$\varphi_s = \omega_e t + 2 \arctan\left(-\frac{K_0 - i\kappa \tan\left(\frac{1}{2}(t + c_1) i\kappa\right)}{\delta_{e0}}\right).$$

If we take the limit when t goes to infinity for the arctan term we have

$$\lim_{t \rightarrow \infty} \arctan\left(\frac{K_0 - i\kappa \tan\left(\frac{1}{2}(t + c_1) i\kappa\right)}{\omega_e - \omega_0}\right) = \arctan\left(\frac{K_0 + \kappa}{\omega_e - \omega_0}\right),$$

or

$$\arctan\left(\frac{K_0 + \sqrt{K_0^2 - (\omega_0 - \omega_e)^2}}{\omega_e - \omega_0}\right).$$

If $K_0 \gg |\omega_0 - \omega_e|$, then

$$\begin{aligned} \lim_{t \rightarrow \infty} \arctan\left(\frac{K_0 - i\kappa \tan\left(\frac{1}{2}(t + c_1) i\kappa\right)}{\omega_e - \omega_0}\right) &\approx \arctan\left(\frac{2K_0}{\omega_e - \omega_0}\right) \\ &\approx \pm \frac{\pi}{2}. \end{aligned}$$

So, for large K_0 and t ,

$$\varphi_s \approx \omega_e t \pm \pi$$

and

$$\varphi_{r_1} \approx \omega_e t \pm \pi.$$

We now turn to

$$\dot{\varphi}_{r_2} = \omega_0 + K_0 \sin(\varphi_{r_2} - \omega_e t - \pi).$$

The solution is

$$\varphi_{r_2} = \omega_e t - 2 \arctan\left(\frac{\Gamma'}{\delta_{e0}}\right),$$

where $\Gamma' = K_0 + \sqrt{\delta_{e0}^2 - K_0^2} \tan\left(\frac{1}{2}(t + c_2)\sqrt{\delta_{e0}^2 - K_0^2}\right)$, and following the same arguments as before, we obtain

$$\lim_{t \rightarrow \infty} \arctan\left(\frac{K_0 + i\kappa \tan\left(\frac{1}{2}(t + c_2) i\kappa\right)}{\omega_e - \omega_0}\right) \approx \arctan(0) \approx 0,$$

or, for large K_0 and t ,

$$\varphi_{r_2} \approx \omega_e t.$$

Of course, the above arguments only tell us the behavior of the equations when t goes to infinity, but in our models we deal with finite times. To better understand how fast the solution converges to $\omega_e t \pm \pi$ or $\omega_e t$, let us rewrite equation

$$\varphi_s = \omega_e t + 2 \arctan\left(-\frac{\Gamma}{\delta_{e0}}\right)$$

in terms of dimensionless quantities. Let $\gamma = (\omega_e - \omega_0)/K_0$, then

$$\begin{aligned} \varphi_s &= \omega_e t \\ &+ 2 \arctan\left(\frac{1}{\gamma} \left[1 - \sqrt{\gamma^2 - 1} \tan\left(\frac{1}{2}(t + c_1) K_0 \sqrt{\gamma^2 - 1}\right)\right]\right). \end{aligned}$$

Since γ is real and $\gamma \ll 1$ for large values of K_0 , we rewrite

$$\begin{aligned} \varphi_s &= \omega_e t \\ &+ 2 \arctan\left(\frac{1}{\gamma} \left[1 + \sqrt{1 - \gamma^2} \tanh\left(\frac{K_0}{2}(t + c_1) \sqrt{1 - \gamma^2}\right)\right]\right). \end{aligned}$$

We're only interested in the last term. We define

$$A = 2 \arctan\left(\frac{1 + \sqrt{1 - \gamma^2} \tanh\left(\frac{K_0}{2}(t + c_1) \sqrt{1 - \gamma^2}\right)}{\gamma}\right). \quad (\text{Appendix B.7})$$

But

$$\tanh \frac{K_0 (t + c_1) \sqrt{1 - \gamma^2}}{2} = \frac{e^{\frac{K_0}{2}(t+c_1)\sqrt{1-\gamma^2}} - e^{-\frac{K_0}{2}(t+c_1)\sqrt{1-\gamma^2}}}{e^{\frac{K_0}{2}(t+c_1)\sqrt{1-\gamma^2}} + e^{-\frac{K_0}{2}(t+c_1)\sqrt{1-\gamma^2}}}, \quad (\text{Appendix B.8})$$

and for large values of t it goes to 1. In fact, (Appendix B.8), and therefore (Appendix B.7), shows a characteristic time

$$t_c = \frac{2}{K_0 \sqrt{1 - \gamma^2}} = \frac{2}{\sqrt{K_0^2 - (\omega_e - \omega_0)^2}}.$$

Thus, for $t > t_c$ and for large K_0 (i.e., $K_0 \gg |\omega_e - \omega_0|$), a good approximation for φ_s is

$$\varphi_s \approx \omega_e t \pm \pi.$$

Similar arguments can be made for φ_{r_1} and φ_{r_2} .

Appendix C. Appendix - Effectiveness of Reinforcement

Here we show how to compute K' from the behavioral parameter c and the other oscillator parameters. First, K_0 satisfies the normal distribution density

$$p(K_0) = \frac{1}{\sigma \sqrt{2\pi}} e^{-\frac{1}{2\sigma^2}(K_0 - \bar{K}_0)^2}, \quad (\text{Appendix C.1})$$

where σ is the standard deviation. The sigmoid function

$$\epsilon(K_0) = \frac{\epsilon_0}{1 + e^{-\gamma(K_0 - K')}} \quad (\text{Appendix C.2})$$

determines whether the couplings are affected. We also assume that the time of reinforcement, Δt_e , is large compared to $1/\epsilon$, as discussed in the text. If $\gamma \gg 1$, $\epsilon(K_0)$ approaches a Heaviside function $\theta(K_0)$ as $\epsilon(K_0) \approx \epsilon_0 \theta(K_0 - K')$. Thus, for large values of γ , learning happens only if $K_0 > K'$, and the probability of an oscillator reinforcement being effective (given that all other parameters are adequately chosen, as discussed in the article), called c , is

$$c = \frac{1}{\sigma \sqrt{2\pi}} \int_{K'}^{\infty} e^{-\frac{1}{2\sigma^2}(K_0 - \bar{K}_0)^2} dK_0, \quad (\text{Appendix C.3})$$

or

$$c = \frac{1}{2} \left(1 + \operatorname{erf} \left(\frac{\sqrt{2} \bar{K}_0 - K'}{2\sigma} \right) \right). \quad (\text{Appendix C.4})$$

Since c is monotonically decreasing with K' , it is possible to solve the above equation for K' . For example, if we set $c' = .19$ we obtain that

$$\overline{K}_0 - K' = -0.8779\sigma. \quad (\text{Appendix C.5})$$

Choosing $\sigma = 10$ and $\overline{K}_0 = 100$, from (Appendix C.5) we obtain $K' = 187.79$.

Appendix D. Appendix - Fixed points for coding phase relations

From $\varphi_s = \omega_e t$, $\varphi_{r_1} = \omega_e t + \delta\varphi$, and $\varphi_{r_2} = \omega_e t + \delta\varphi - \pi$ and (37)–(39) we obtain the following fixed points for excitatory connections, which work as an attractor for the asymptotic behavior.

$$\begin{aligned} k_{s,r_1}^E &= \alpha \cos(\delta\varphi), \\ k_{s,r_2}^E &= -\alpha \cos(\delta\varphi), \\ k_{r_1,r_2}^E &= -\alpha, \\ k_{r_1,s}^E &= \alpha \cos(\delta\varphi), \\ k_{r_2,s}^E &= -\alpha \cos(\delta\varphi), \\ k_{r_2,r_1}^E &= -\alpha. \end{aligned}$$

Similarly, for inhibitory connections we have.

$$\begin{aligned} k_{s,r_1}^I &= -\alpha \sin(\delta\varphi), \\ k_{s,r_2}^I &= \alpha \sin(\delta\varphi), \\ k_{r_1,r_2}^I &= 0, \\ k_{r_1,s}^I &= \alpha \sin(\delta\varphi), \\ k_{r_2,s}^I &= -\alpha \sin(\delta\varphi), \\ k_{r_2,r_1}^I &= 0. \end{aligned}$$

Kuramoto's equations become

$$\begin{aligned}
\frac{d\varphi_s}{dt} &= \omega_0 - \alpha \cos(\delta\varphi) \sin(\varphi_s - \varphi_{r_1}) \\
&\quad + \alpha \cos(\delta\varphi) \sin(\varphi_s - \varphi_{r_2}) \\
&\quad + \alpha \sin(\delta\varphi) \cos(\varphi_s - \varphi_{r_1}) \\
&\quad - \alpha \sin(\delta\varphi) \cos(\varphi_s - \varphi_{r_2}), \\
\frac{d\varphi_{r_1}}{dt} &= \omega_0 - \alpha \cos(\delta\varphi) \sin(\varphi_{r_1} - \varphi_s) \\
&\quad + \alpha \sin(\varphi_{r_1} - \varphi_{r_2}) \\
&\quad - \alpha \sin(\delta\varphi) \cos(\varphi_{r_1} - \varphi_s), \\
\frac{d\varphi_{r_2}}{dt} &= \omega_0 + \alpha \cos(\delta\varphi) \sin(\varphi_{r_2} - \varphi_s) \\
&\quad + \alpha \sin(\varphi_{r_2} - \varphi_{r_1}) \\
&\quad + \alpha \sin(\delta\varphi) \cos(\varphi_{r_2} - \varphi_s).
\end{aligned}$$

Regrouping the terms with same phase oscillators, we have

$$\begin{aligned}
\frac{d\varphi_s}{dt} &= \omega_0 - \alpha \sin(\varphi_s - \varphi_{r_1} + \delta\varphi) \\
&\quad + \alpha \sin(\varphi_s - \varphi_{r_2} + \delta\varphi), \\
\frac{d\varphi_{r_1}}{dt} &= \omega_0 - \alpha \sin(\varphi_{r_1} - \varphi_s - \delta\varphi) \\
&\quad + \alpha \sin(\varphi_{r_1} - \varphi_{r_2}), \\
\frac{d\varphi_{r_2}}{dt} &= \omega_0 + \alpha \sin(\varphi_{r_2} - \varphi_s - \delta\varphi) \\
&\quad + \alpha \sin(\varphi_{r_2} - \varphi_{r_1}),
\end{aligned}$$

or

$$\begin{aligned}
\frac{d\varphi_s}{dt} &= \omega_0 - \alpha \sin(\varphi_s - \varphi_{r_1} + \delta\varphi) \\
&\quad - \alpha \sin(\varphi_s - \varphi_{r_2} + \delta\varphi - \pi), \\
\frac{d\varphi_{r_1}}{dt} &= \omega_0 - \alpha \sin(\varphi_{r_1} - \varphi_s - \delta\varphi) \\
&\quad - \alpha \sin(\varphi_{r_1} - \varphi_{r_2} - \pi), \\
\frac{d\varphi_{r_2}}{dt} &= \omega_0 - \alpha \sin(\varphi_{r_2} - \varphi_s - \delta\varphi + \pi) \\
&\quad - \alpha \sin(\varphi_{r_2} - \varphi_{r_1} + \pi),
\end{aligned}$$

which codes exactly the phase relations we were seeking.

Appendix E. Appendix - Pseudomaximum Likelihood Estimates

For the pseudomaximum likelihood estimates, we follow Suppes and Atkinson (1960). We want to compute the pseudomaximum likelihood based on the following asymptotic conditional probabilities (from Eqs. **10.6.6** and **10.6.7** in Suppes and Atkinson (1960, Chapter 10)).

$$P_{\infty}(R_{1,n+1}|E_{1,n}R_{1,n}) = \beta + \frac{1-\beta}{N},$$

$$P_{\infty}(R_{1,n+1}|E_{1,n}R_{2,n}) = \beta\left(1 - \frac{1}{N}\right) + \frac{c}{N},$$

$$P_{\infty}(R_{1,n+1}|E_{2,n}R_{1,n}) = \beta\left(1 - \frac{1}{N}\right) + \frac{1-c}{N},$$

$$P_{\infty}(R_{1,n+1}|E_{2,n}R_{2,n}) = \beta\left(1 - \frac{1}{N}\right),$$

$$P_{\infty}(R_{2,n+1}|E_{1,n}R_{1,n}) = 1 - \beta - \frac{1-\beta}{N},$$

$$P_{\infty}(R_{2,n+1}|E_{1,n}R_{2,n}) = 1 - \beta\left(1 - \frac{1}{N}\right) - \frac{c}{N},$$

$$P_{\infty}(R_{2,n+1}|E_{2,n}R_{1,n}) = 1 - \beta\left(1 - \frac{1}{N}\right) - \frac{1-c}{N},$$

$$P_{\infty}(R_{2,n+1}|E_{2,n}R_{2,n}) = 1 - \beta\left(1 - \frac{1}{N}\right),$$

where β , $0 \leq \beta \leq 1$, is the probability of noncontingent reinforcement of E_1 and $(1 - \beta)$ the probability of E_2 . Then

$$\begin{aligned}
L(c, N) = & n_{11,1} \log \left[\beta + \frac{1 - \beta}{N} \right] \\
& + n_{21,1} \log \left[\beta \left(1 - \frac{1}{N} \right) + \frac{c}{N} \right] \\
& + n_{12,1} \log \left[\beta \left(1 - \frac{1}{N} \right) + \frac{1 - c}{N} \right] \\
& + n_{22,1} \log \left[\beta \left(1 - \frac{1}{N} \right) \right] \\
& + n_{11,2} \log \left[1 - \beta - \frac{1 - \beta}{N} \right] \\
& + n_{21,2} \log \left[1 - \beta \left(1 - \frac{1}{N} \right) - \frac{c}{N} \right] \\
& + n_{12,2} \log \left[1 - \beta \left(1 - \frac{1}{N} \right) - \frac{1 - c}{N} \right] \\
& + n_{22,2} \log \left[1 - \beta \left(1 - \frac{1}{N} \right) \right].
\end{aligned}$$

We use the above function to compute, using Maple 10, the values of c that maximize it for $N = 2$, $N = 3$, and $N = 4$, as well as to compute the maximum of the function for c and N , estimating the best \hat{N} that fits the following data (extracted from equations **10.6.8**, Suppes and Atkinson (1960, Chapter 10)). In our notation below, $n_{ij,k}$ is the transition frequency from R_i and E_j on trial n to R_k on trial $n + 1$. Then, $n_{11,1} = 748$, $n_{11,2} = 298$, $n_{12,1} = 394$, $n_{12,2} = 342$, $n_{21,1} = 462$, $n_{21,2} = 306$, $n_{22,1} = 186$, and $n_{22,2} = 264$. The results are the following. For the two element model, we have $\hat{c}_2 = 0.5675$. For the three-element model, we have $\hat{c}_3 = 0.5996$. For the four-element model we have $\hat{c}_4 = 0.6314$. Finally, maximizing L for both c and N we obtain $\hat{c} = 0.6106$ and $\hat{N} = 3.35$.

References

Acebron, J. A., Bonilla, L. L., Vicente, C. J. P., Ritort, F., Spigler, R., 2005. The kuramoto model: A simple paradigm for synchronization phenomena. *Reviews of Modern Physics* 77 (1), 137–185.

- Bower, G., 1961. Application of a model to paired-associate learning. *Psychometrika* 26, 255–280.
- Bower, J. M., Beeman, D., 2003. The Book of Genesis: Exploring Realistic Neural Models with the GEneral NEural Simulation System. Internet Edition.
URL <http://www.genesis-sim.org/GENESIS>
- Bruza, P., Busemeyer, J., Gabora, L., 2009. Introduction to the special issue on quantum cognition. *Journal of Mathematical Psychology* 53, 303–305.
- de Barros, J. A., Carvalhaes, C. G., de Mendonca, J. P. R. F., Suppes, P., 2006. Recognition of words from the eeg laplacian. *Revista Brasileira de Engenharia Biomedica* 21, 45–59.
- de Barros, J. A., Suppes, P., 2009. Quantum mechanics, interference, and the brain. *Journal of Mathematical Psychology* 53, 306–313.
- Eckhorn, R., Bauer, R., Jordan, W., Brosch, M., Kruse, W., Munk, M., Reitboeck, H., 1988. Coherent oscillations: A mechanism of feature linking in the visual cortex? *Biological Cybernetics* 60 (2), 121–130.
- Eeckman, F. H., Freeman, W. J., 1991. Asymmetric sigmoid non-linearity in the rat olfactory system. *Brain Research* 557, 13–21.
- Ermentrout, G. B., Kleinfeld, D., 2001. Traveling electrical waves in cortex: insights from phase dynamics and speculation on a computational role. *Neuron* 29 (1), 33–44.
- Estes, W., Suppes, P., Bush, R., Estes, W., 1959. Studies in mathematical learning theory. Stanford University Press Stanford.
- Estes, W. K., Suppes, P., 1959. Foundations of linear models. In: Bush, R. R., Estes, W. K. (Eds.), *Studies in Mathematical Learning Theory*. Stanford University Press, Stanford, CA, pp. 137–179.

- Fell, J., Klaver, P., Lehnertz, K., Grunwald, T., Schaller, C., Elger, C. E., Fernandez, G., 2001. Human memory formation is accompanied by rhinal-hippocampal coupling and decoupling. *Nature neuroscience* 4 (12), 1259–1264.
- Freeman, W. J., 1979. Nonlinear dynamics of paleocortex manifested in the olfactory eeg. *Biological Cybernetics* 35, 21–37.
- Freeman, W. J., Barrie, J. M., 1994. Temporal Coding in the Brain. Springer, New York, Ch. Chaotic oscillations and the genesis of meaning in cerebral cortex, pp. 13–37, corrected Internet edition, available at <http://sulcus.berkeley.edu/wjf/AB.Genesis.of.Meaning.pdf>.
- Friedrich, R. W., Habermann, C. J., Laurent, G., 2004. Multiplexing using synchrony in the zebrafish olfactory bulb. *Nature neuroscience* 7 (8), 862–871.
- Gerstner, W., Kistler, W., 2002. Spiking Neuron Models. Cambridge University Press, Cambridge.
- Guckenheimer, J., Holmes, P., 1983. Nonlinear Oscillations, Dynamical Systems, and Bifurcation of Vector Fields. Springer-Verlag, New York.
- Hoppensteadt, F. C., Izhikevich, E. M., 1996a. Synaptic organizations and dynamical properties of weakly connected neural oscillators i. analysis of a canonical model. *Biological Cybernetics* 75 (2), 117–127.
- Hoppensteadt, F. C., Izhikevich, E. M., 1996b. Synaptic organizations and dynamical properties of weakly connected neural oscillators ii. learning phase information. *Biological Cybernetics* 75 (2), 129–135.
- Izhikevich, E. M., 2007. Dynamical Systems in Neuroscience: The Geometry of Excitability and Bursting. The MIT Press, Cambridge, Massachusetts.
- Izhikevich, E. M., Kuramoto, Y., 2006. Weakly coupled oscillators. In: *Encyclopedia of Mathematical Physics*. Elsevier.

- Kazantsev, V. B., Nekorkin, V. I., Makarenko, V. I., Llinas, R., 2004. Self-referential phase reset based on inferior olive oscillator dynamics. *Proceedings of the National Academy of Sciences of the United States of America* 101 (52), 18183–18188.
- Kuramoto, Y., 1984. *Chemical Oscillations, Waves, and Turbulence*. Dover Publications, Inc., Mineola, New York.
- Leznik, E., Makarenko, V., Llinas, R., 2002. Electrotonically Mediated Oscillatory Patterns in Neuronal Ensembles: An In Vitro Voltage-Dependent Dye-Imaging Study in the Inferior Olive. *J. Neurosci.* 22 (7), 2804–2815.
- Luce, R. D., 1986. *Response Times*. Oxford University Press, New York.
- Lutz, A., Lachaux, J.-P., Martinerie, J., Varela, F. J., 2002. Guiding the study of brain dynamics by using first-person data: Synchrony patterns correlate with ongoing conscious states during a simple visual task. *Proceedings of the National Academy of Sciences* 99 (3), 1586–1591.
- Lytton, W. W., Sejnowski, T. J., 1991. Simulations of cortical pyramidal neurons synchronized by inhibitory interneurons. *J Neurophysiol* 66 (3), 1059–1079.
- Murthy, V. N., Fetz, E. E., 1992. Coherent 25- to 35-Hz Oscillations in the Sensorimotor Cortex of Awake Behaving Monkeys. *Proceedings of the National Academy of Sciences* 89 (12), 5670–5674.
- Nishii, J., 1998. A learning model for oscillatory networks. *Neural Networks* 11 (2), 249–257.
- Park, E.-H., Soa, P., Barreto, E., Gluckman, B. J., Schi, S. J., 2003. Electric field modulation of synchronization in neuronal networks. *Neurocomputing* 52-54, 169–175.
- Rees, G., Kreiman, G., Koch, C., 2002. Neural correlates of consciousness in humans. *Nat Rev Neurosci* 3 (4), 261–270.

- Rodriguez, E., George, N., Lachaux, J.-P., Martinerie, B. R., Varela, F. J., 1999. Perception's shadow: long-distance synchronization of human brain activity. *Nature* 397, 430–433.
- Seliger, P., Young, S. C., Tsimring, L. S., 2002. Plasticity and learning in a network of coupled phase oscillators. *Physical Review E* 65, 041906–1–7.
- Sompolinsky, H., Golomb, D., Kleinfeld, D., 1990. Global Processing of Visual Stimuli in a Neural Network of Coupled Oscillators. *PNAS* 87 (18), 7200–7204.
- Steinmetz, P. N., Roy, A., Fitzgerald, P. J., Hsiao, S. S., Johnson, K. O., Niebur, E., 2000. Attention modulates synchronized neuronal firing in primate somatosensory cortex. *Nature* 404 (6774), 187–190.
- Strogatz, S. H., 2000. From kuramoto to crawford: exploring the onset of synchronization in populations of coupled oscillators. *Physica D: Nonlinear Phenomena* 143 (1–4), 1–20.
- Suppes, P., 1959. Stimulus sampling theory for a continuum of responses. Institute for Mathematical Studies in the Social Sciences, Applied Mathematics and Statistics Laboratories, Stanford University, Stanford, Calif.
- Suppes, P., 2002. Representation and Invariance of Scientific Structures. CSLI Publications, Stanford, CA.
- Suppes, P., Atkinson, R. C., 1960. Markov Learning Models for Multiperson Interactions. Stanford University Press, Stanford, CA.
- Suppes, P., de Barros, J. A., 2007. Quantum mechanics and the brain. In: *Quantum Interaction: Papers from the AAAI Spring Symposium*. Technical Report SS-07-08. AAAI Press, Menlo Park, CA, pp. 75–82.
- Suppes, P., Frankmann, R., 1961. Test of stimulus sampling theory for a continuum of responses with unimodal noncontingent determinate reinforcement. *Journal of Experimental Psychology* 61 (2), 122–132.

- Suppes, P., Ginsberg, R., 1963. A fundamental property of all-or-none models, binomial distribution of responses prior to conditioning, with application to concept formation in children. *Psychological Review* 70, 139–161.
- Suppes, P., Han, B., 2000. Brain-wave representation of words by superposition of a few sine waves. *Proceedings of the National Academy of Sciences* 97, 8738–8743.
- Suppes, P., Han, B., Epelboim, J., Lu, Z.-L., 1999a. Invariance between subjects of brain wave representations of language. *Proceedings of the National Academy of Sciences* 96, 12953–12958.
- Suppes, P., Han, B., Epelboim, J., Lu, Z.-L., 1999b. Invariance of brain-wave representations of simple visual images and their names. *Proceedings of the National Academy of Sciences* 96, 14658–14663.
- Suppes, P., Han, B., Lu, Z.-L., 1998. Brain-wave recognition of sentences. *Proceedings of the National Academy of Sciences* 95, 15861–15866.
- Suppes, P., Lu, Z.-L., Han, B., 1997. Brain wave recognition of word. *Proceedings of the National Academy of Sciences* 94, 14965–14969.
- Suppes, P., Rouanet, H., Levine, M., Frankmann, R., 1964a. Empirical comparison of models for a continuum of responses with noncontingent bimodal reinforcement. *Studies in mathematical psychology*, 358–379.
- Suppes, P., Rouanet, H., Levine, M., Frankmann, R. W., 1964b. Empirical comparison of models for a continuum of responses with noncontingent bimodal reinforcement. In: Atkinson, R. C. (Ed.), *Studies in Mathematical Psychology*. Stanford University Press, Stanford, CA, pp. 358–379.
- Tallon-Baudry, C., Bertrand, O., Fischer, C., 2001. Oscillatory Synchrony between Human Extrastriate Areas during Visual Short-Term Memory Maintenance. *J. Neurosci.* 21 (20), 177RC–1–5.
- Trevisan, M. A., Bouzat, S., Samengo, I., Mindlin, G. B., 2005. Dynamics of learning in coupled oscillators tutored with delayed reinforcements. *Physical Review E (Statistical, Nonlinear, and Soft Matter Physics)* 72 (1), 011907–1–7.

- Varela, F., Lachaux, J.-P., Rodriguez, E., Martinerie, J., 2001. The brainweb: phase synchronization and large-scale integration. *Nature reviews. Neuroscience* 2 (4), 229–239.
- Wang, D., 1995. Emergent synchrony in locally coupled neural oscillators. *Neural Networks, IEEE Transactions on Neural Networks* 6 (4), 941–948.
- Winfree, A. T., 2002. OSCILLATING SYSTEMS: On Emerging Coherence. *Science* 298 (5602), 2336–2337.
- Wong, D. K., Uy, E. T., Guimaraes, M. P., Yang, W., Suppes, P., 2006. Interpretation of perceptron weights as construct time series for eeg classification. *Neurocomputing* In press.
- Wright, J., Liley, D., 1995. Simulation of electrocortical waves. *Biological Cybernetics* 72 (4), 347–356.
- Yamanishi, J.-i., Kawato, M., Suzuki, R., 1980. Two coupled oscillators as a model for the coordinated finger tapping by both hands. *Biological Cybernetics* 37 (4), 219–225.